

# Nonlinear Vibration Characteristics of Virtual Mass Systems for Wind Turbine Blade Fatigue Test

## ~~Nonlinear Vibration Characteristics of Wind Turbine Blades Based on Virtual Mass Match~~

Aiguo Zhou<sup>1</sup>, Jinlei Shi<sup>1</sup>, Tao Dong<sup>1</sup>, Yi Ma<sup>1</sup>, Zhenhui Weng<sup>2</sup>

<sup>1</sup>School of Mechanical Engineering, Tongji University, Shanghai 200082

<sup>2</sup>Aeolon Technology Co., Ltd, Shanghai 200120, China

Correspondence to: Jinlei Shi (shijinlei1430@163.com)

**Abstract.** ~~To analyze the nonlinear effects of the virtual masses used for load decoupling on the vibration characteristics in the biaxial fatigue test of wind turbine blades, the equivalent dynamic model of the blade virtual masses test system is established using the Lagrange method firstly. Then, the nonlinear effects of blade amplitude and installation parameters of virtual masses on the test system are obtained by numerical methods. Moreover, the nonlinear amplitude-frequency characteristics of the test system is analyzed theoretically based on the nonlinear vibration theory. Finally, two blades over 80m are analyzed under the dynamic simulation environment. The results indicate that the resonance frequency of the test system decreases with the increase of the amplitude of the blade, presenting the nonlinear amplitude frequency characteristics. In the case of 80m blade, the resonance frequency of the test system decreases by approximately 2%. There is also a nonlinear relation between the length of the seesaw used to install the virtual masses and the resonance frequency. The decrease of resonance frequency of the test system is more obvious with shorter seesaw, the resonance frequency decreases by up to 1.8% under certain conditions. The decrease of the resonance frequency will also reduce the area of interest for blade load verification, the blade load distribution decreases by nearly 3% in the flap wise direction under the given operating conditions. In addition, the virtual masses will also affect the resonance characteristics and the spatial trajectory of the blade during the biaxial test.~~

The biaxial fatigue test of wind turbine blades is helpful to shorten the test time and is more suitable for the actual operating conditions. Adding tuning masses to the blade is a common method for blade uniaxial test at present, and its purpose is to adjust the load distribution in one direction of the blade. However, the tuning masses on the blade will affect the load distribution in the direction of the blade flap-wise and edge-wise at the same time in the biaxial test, so the concept of "virtual masses" is proposed to realize the decoupling of the load distribution in the biaxial test. Due to the limitation of the size of the virtual masses mechanism and the complex motion trajectory of the blade, the actual inertial effect provided by the virtual masses is different from the ideal situation, which will affect the resonance characteristics of the test system and the load distribution of the blade. Therefore, in order to evaluate the effect of the nonlinear effect introduced by the virtual masses on the resonance characteristics of the test system and the blade load distribution, the equivalent dynamic model of the bladed virtual mass test system was established by using the Lagrange method. Then, the nonlinear effects of blade amplitude and virtual mass installation parameters on the test system are obtained by numerical method. Then, based on the nonlinear vibration theory, the approximate nonlinear amplitude-frequency characteristics of the test system are obtained, that is, the resonance frequency of the test system will decrease with the increase of the blade amplitude. Through the simulation analysis of two 80m+ blades, the applicability of the theoretical method is verified. It can be seen from the simulation results of the simulated uniaxial test that the larger the amplitude of the blade and the shorter the connection rod will reduce the resonance frequency of the test system. When the vibration amplitude at the excitation point is the same, a lower resonance frequency results in a smaller load distribution level, that is, the area which is actually fully tested will be reduced. In the biaxial simulation test, the resonance frequency of the test system will be further reduced because the virtual masses will be affected by the coupled motion in both directions at the same time. Besides, the introduction of an external mechanism of the virtual mass will also cause deformation of the envelope of the blade biaxial trajectory, which will further affect the load distribution of the

43 blade. This work explores the nonlinear influence of virtual mass on the actual fatigue test, provides the corresponding  
44 theoretical basis and reference for the test organization to adjust the tuning masses scheme in advance to adjust the load  
45 distribution and select the exciting equipment.

## 46 **1 Introduction**

47 As an important component of wind turbine, the cost of blades accounts for 20% of the overall machine, so the lifetime  
48 of blades is the premise to ensure safe and stable operation of the wind turbine (Zhang et al., 2015; Liao et al., 2016). To verify  
49 the reliability of the blade under the actual operating field, the International Electrotechnical Commission (IEC) points out that  
50 the full-scale fatigue test of rotor blades is needed to be performed (IEC, 2014). In the actual blade fatigue test, which means  
51 two separate oscillations tests with over one million damage-equivalent loads cycles are performed at the 1st and 2nd natural  
52 frequency of the blade.

53 The fatigue test requires that the load in the area of interest along the blade span-wise direction matches or exceeds the  
54 design value, while keeping the exceedance as small as possible in order to avoid unrealistic failures (DNV GL AS, 2015). To  
55 satisfy the above requirements, additional masses are usually attached to the blade to tune the test load distribution which needs  
56 to be optimized by determining the optimal mass masses distribution.

57 To save testing time and to emulate the comprehensive damage along the circumference of the blade, several institutions  
58 began to study and design biaxial fatigue test (White et al., 2004; Greaves et al., 2012; Snowberg et al., 2014; Hughes et al.,  
59 1999; Liao et al., 2014;), namely to excites the blade in both directions simultaneously. In the previous resonance biaxial test,  
60 a reasonable load distribution (in both directions) will be obtained by optimizing the position and tuning masses installed  
61 on the blade. However, the tuning masses installed on the blade will affect the vibration characteristics (mode shape and  
62 frequency) in both flap-wise and edge-wise directions, which brings difficulty to the biaxial load match optimization,  
63 and there may be excessive overload in a certain area of the blade when choosing a compromise.

64 To simplify load match, the extra mechanism makes the tuning masses only act in one vibration direction (called  
65 virtual masses), and the biaxial load match is equivalent to the combination of the load match of two single axis test.  
66 The purpose of the virtual masses is to decouple the biaxial load, so that the biaxial load match is equivalent to the  
67 combination of the load match of two single axis test. Compared with the uniaxial fatigue test, the biaxial fatigue test has  
68 more complicated masses matching. Because the additional masses will affect the load distribution in both directions  
69 simultaneously, which is called as masses coupling. To solve the problem of masses coupling in the biaxial fatigue test, some  
70 test institutions introduce the concept of virtual masses. Post et al. (2016) firstly proposed the concept of virtual masses to  
71 tune both natural frequencies independently in the two directions, and to eliminate the coupling phenomenon of test  
72 bending moments during biaxial test. Melcher et al. (2020<sub>a</sub>, 2021<sub>2020b</sub>) used elastic elements to adjust blade stiffness,  
73 and optimized biaxial fatigue test parameters based on virtual masses and elastic elements. Zhang et al. (2020) and Lu  
74 et al. (2022) carried out research on biaxial load matching and design using virtual masses. The virtual masses used for  
75 mass decoupling is ideally regarded as translational motion and the push rod between the virtual mass and the blade is  
76 always in line with the main vibration in the above work ~~The above research work regards the virtual masses used for~~  
77 ~~masses decoupling as translational motion~~, which is difficult to apply to the actual test field. Because a larger and stronger  
78 platform is needed to keep virtual mass translate in the edge-wise direction, which is difficult to achieve in a limited test  
79 space. In the biaxial test, the platform may interfere with the push rod, especially when the blade has a large amplitude  
80 in the flap-wise direction. ~~Because it requires large equipment and is difficult to apply to the test condition of large blade~~  
81 ~~vibration.~~ Therefore, IWES conducted further research, designed a device to convert virtual masses from translation to  
82 rotation, and applied it to the biaxial fatigue test which has a frequency ratio of 1:1 (Melcher et al., 2020<sub>c</sub>). Further, the  
83 feasibility of the biaxial decoupling test of the bending moment was verified by the comparison of simulation and  
84 experiment results (Melcher et al., 2020; Castro et al., 2021; Falko et al., 2020; Falko et al., 2020; Castro et al., 2021). In  
85 fact, in the view of the motion characteristics, the inertia force generated by rotating virtual masses is different from that  
86 generated by translational virtual masses. Taking a uniaxial test as an example, the translational virtual masses move  
87 synchronously with the blade, which behave like a mass acting in just one direction from a numerical standpoint. The

88 translational virtual masses have the same motion characteristics as the additional tuning masses. Therefore, although  
89 the virtual mass is not on the blade, the inertia force generated by it and the inertia force generated by the additional  
90 tuning masses are in the same direction and magnitude. The rotating virtual masses are limited by the constraints of the  
91 seesaw, and its motion path is the rotating motion around the center of the seesaw. Therefore, the direction and magnitude  
92 of the inertial force generated by the rotation of the virtual mass will change, and it is not equivalent to the translational  
93 virtual masses. However, changes in the inertia force provided by the virtual masses will cause changes in the  
94 characteristics of the system, which may further cause changes in the blade load distribution, and may put forward higher  
95 requirements for vibration excitation equipment.

96 To reveal the vibration mechanism of the blade-virtual masses test system and provide a more rigorous theoretical basis  
97 for the biaxial load matching theory of the blade. In this paper, a theoretical model of blade-virtual masses uniaxial test system  
98 is established. The specific nonlinear impact of single parameter related to virtual masses on the characteristics of the test  
99 system can be obtained intuitively through the uniaxial model. Then, two blades over 80m were simulated in ADAMS. Uniaxial  
100 simulation was used to verify the applicability of the theoretical model, including the nonlinear amplitude-frequency  
101 characteristics of the system and the effects of virtual mass installation parameters (such as seesaw length) on the load  
102 distribution of the blade. Biaxial simulation is used to analyze the nonlinear effect of virtual mass on the system under the  
103 simultaneous action of many factors. This work will be used in the future research to adopt reasonable control strategy and  
104 adjust the counterweight scheme in advance to achieve the target damage of the blade. This work establishes the dynamic  
105 model of the blade-virtual masses test system and analyses the nonlinear amplitude-frequency characteristics of the test system.  
106 The aim is to further analyze the effects of rotating virtual masses on the blade test system, and to reveal the vibration  
107 mechanism of the blade-virtual masses test system to provide a more rigorous theoretical basis for the biaxial load matching  
108 theory of the blade. Moreover, two blades over 80m were simulated to verify the nonlinear vibration characteristics of the test  
109 system and evaluate the effects of installation parameters of virtual masses on blade test load distribution, such as the length  
110 of the seesaw.

## 111 2 Blade-virtual masses equivalent dynamic model

112 The ~~tuning~~additional masses can change the modal characteristics of the testing system to adjust the test load distribution of  
113 the blade, which is essentially bending moment caused by the inertia force brought by the reciprocating motion of the self-  
114 weight and additional masses. In the common fatigue test system, the additional masses are directly attached to the blade, as  
115 shown in Fig. 1 (a). When the ~~tuning~~additional masses are determined, the modal characteristics of the testing system are  
116 basically determined, as shown in Fig. 1 (a). This means that, without considering the air damping, the resonant frequency of  
117 the system remains unchanged.

118 In the biaxial fatigue test, the ~~tuning~~additional ~~mass~~decouples masses decouple the biaxial load by seesaw, and the  
119 ~~tuning~~additional masses are is-called virtual masses, as shown in Fig. 1 (b). In this installation condition, the inertia force  
120 generated by the virtual masses mainly only acts in the edge-wise direction in Fig. 1 (b) of an individual blade mode. The  
121 mechanism for mounting the virtual ~~mass~~masses consists of a push rod and a seesaw. The ~~push rod~~, blade fixture, push rod,  
122 and seesaw are connected through a universal joint, and the seesaw can rotate around the center position. Tuning massesMasses  
123 are located at both ends of the seesaw to offset each other's gravity. After the exciting force is applied to the blade, the tuning  
124 masses move with the blade and rotate around the center of the seesaw to provide the inertia force for the blade through the  
125 push rod. However, due to the motion characteristics of the virtual ~~mass~~masses mechanism, the motion of the virtual  
126 ~~mass~~masses cannot be perfectly synchronized with the blade motion. Therefore, the inertia force generated by the rotation of  
127 the virtual ~~mass~~masses differs from the inertia force generated by the traditional tuning masses. To ~~precisely~~ evaluate the  
128 specific impacts of single parameter related to virtual masses on the test system virtual mass rotation on the blade test system,  
129 it is necessary to establish a corresponding uniaxial theoretical model for analysis from the perspective of control variable

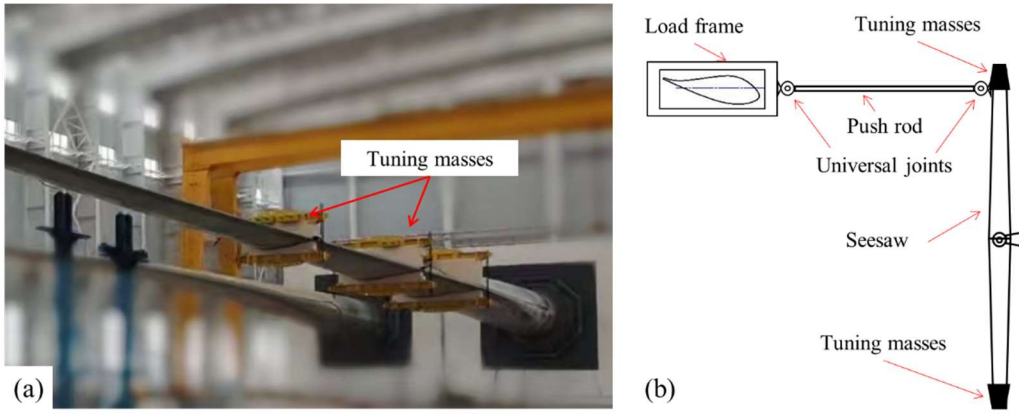


Figure 1: Masses match of blade fatigue test: (a) traditional tuning masses setup (b) virtual masses setup.

### 2.1 The comparison on the amplitude of inertia force

The uniaxial test is taken as an example to illustrate the difference between virtual masses translation and rotation, as shown in Fig.2. The inertial force generated by rotating virtual masses of the blade at the maximum amplitude can be analyzed, as shown in Fig.3. The relationship of the motion between virtual masses and blade can be obtained:

$$\begin{cases} \mathbf{v}_m = \mathbf{v}_M + \mathbf{v}_{mM} \\ \mathbf{a}_m = \mathbf{a}_m^n + \mathbf{a}_m^r = \mathbf{a}_M + \mathbf{a}_{mM}^n + \mathbf{a}_{mM}^r \end{cases} \quad (1)$$

Where:  $\mathbf{v}_m$  - velocity of virtual masses;  $\mathbf{v}_M$  - velocity of blade equivalent mass;  $\mathbf{v}_{mM}$  - relative velocity;  $\mathbf{a}_{mM}^n$  - relative normal acceleration;  $\mathbf{a}_m$  - the acceleration of the virtual masses;  $\mathbf{a}_{mM}^r$  - relative tangential acceleration;  $\mathbf{a}_m^n$  - normal acceleration;  $\mathbf{a}_m^r$  - tangential acceleration.

The blade at the maximum amplitude satisfies:  $\mathbf{v}_M = 0$ ;  $\mathbf{v}_{mM} = 0$ ;  $\mathbf{a}_{mM}^n = 0$ ;  $\mathbf{a}_m^n = 0$ .

The angular acceleration of the virtual mass at the maximum amplitude of the blade can be obtained:

$$|\alpha_m| = \frac{\omega^2 Y \cos(\beta_0)}{R \cos(\theta_0 - \beta_0)} \quad (2)$$

Where:  $\theta$  - Rotation angle of the seesaw at the maximum amplitude of the blade;  $\beta_0$  - Angle between the push rod and the main vibration direction at the maximum amplitude of the blade;  $\alpha_m$  - Angular acceleration of the virtual mass at the maximum amplitude of the blade.

According to Eqs. (1) and Eqs. (2), the rotating inertia force  $F_R$  generated by the rotating virtual mass at the maximum amplitude of the blade can be obtained:

$$F_R = \frac{m\omega^2 Y \cos(\beta_0)}{\cos(\theta_0 - \beta_0)} \quad (3)$$

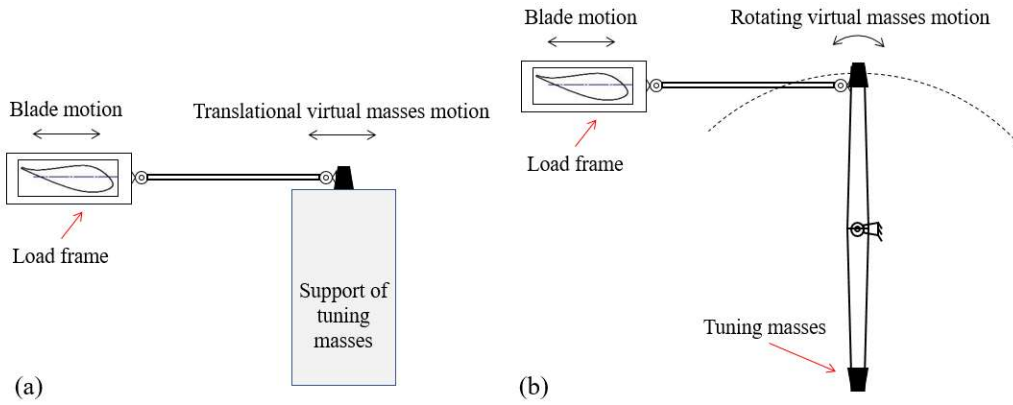
The inertia force  $F_{rot}$  transmitted to the main vibration direction of the blade through the push rod can be obtained:

$$F_{rot} = \frac{F_R \cos(\beta_0)}{\cos(\theta_0 - \beta_0)} = \frac{m\omega^2 Y \cos^2(\beta_0)}{\cos^2(\theta_0 - \beta_0)} \quad (4)$$

The translational virtual masses are consistent with the motion state of the blade, so the inertial force generated by the translational virtual masses can be obtained based on Eqs. (4):

$$F_{tra} = m\omega^2 Y \quad (5)$$

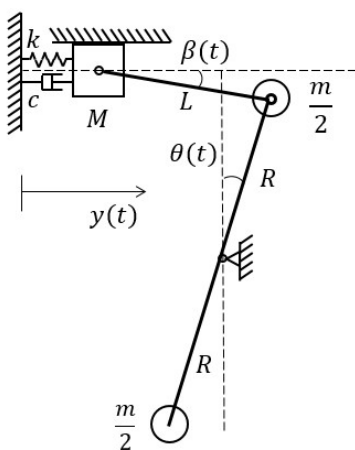
According to Eqs. (4) and Eqs. (5), there are differences in the inertial forces acting on the blades by the two setups, which are mainly caused by the difference in the movement trajectory of masses.



157  
158 **Figure 2: The comparison on inertia force: (a) Translational virtual masses setup (b) Rotating virtual masses setup.**

159 **2.2 Model using the Lagrange method**

160 The aim of virtual masses is to decouple the test load in the biaxial fatigue test. In fact, there will be inertial force coupling in  
 161 the actual biaxial testing process (virtual masses translation or rotation), which will cause multiple factors to work together  
 162 and make it difficult to analyze the system characteristics. Therefore, it is desirable to choose the uniaxial test to analyze the  
 163 nonlinear influence introduced by the virtual masses, which does not mean that the biaxial test can be regarded as the linear  
 164 superposition of the uniaxial test. Essentially, the load distribution in the main vibration direction of the blade is adjusted by  
 165 the component of the inertia force transmitted by the push rod in this direction. Because of the angle between the push rod  
 166 direction and the vibration direction, blade displacement is not in line with the push rod. the motion of the virtual mass  
 167 generates an inertial force that is transmitted to the blades through push rods, thereby adjusting the load distribution in the  
 168 main vibration direction. To more intuitively analyze the impact of virtual mass masses on the blade test system, the mass of  
 169 the push rod and the seesaw are ignored in modeling according to the control variable method, and only their geometric  
 170 dimensions are considered. Take taking the example of blade edge-wise direction test, the blade model is simplified as shown  
 171 in Fig. 23. Moreover, the inertial force of the virtual masses also affects the flap-wise direction of the blade. However, since  
 172 the frequency of the inertial force is close to the first order modal frequency in edge-wise direction, the perturbation to the  
 173 flap-wise direction is relatively small. Therefore, only the influence of virtual mass masses on the vibration characteristics in  
 174 the main testing direction needs to be considered during the uniaxial test. Section 2.1 only analyzes the difference of inertial  
 175 force amplitude in Fig. 2 and this section set up a uniaxial theoretical model to evaluate the effect of virtual masses rotation  
 176 on the vibration characteristics of the test system. In this paper, the Lagrange method is used to analyze the uniaxial model  
 177 (Liu et al., 2019). The initial state of the test system is assumed when the blade is stationary, the push rod is horizontal and the  
 178 seesaw is vertical.



179  
180 **Figure 23: Virtual masses setup for blade fatigue test.**

$$\frac{d}{dt} \left( \frac{\partial T}{\partial \dot{q}_j} \right) - \frac{\partial T}{\partial q_j} + \frac{\partial V}{\partial q_j} + \frac{\partial D}{\partial \dot{q}_j} = Q_j, j = 1, 2, \dots, n \quad (16)$$

Where:  $T$ - kinetic energy;  $V$ - potential energy;  $D$ - dissipated energy;  $q_j$ - generalized coordinate;  $\dot{q}_j$  - generalized velocity;  $Q_j$  - generalized force.

By selecting the generalized coordinate  $q = y$ , and based on the motion relationship in Fig. 23, the displacement and velocity relationships of the test system can be obtained:

$$\begin{cases} y + L \cos \beta - R \sin \theta = L \\ L \sin \beta + R \cos \theta = R \end{cases} \quad (27)$$

$$\begin{cases} \dot{y} - L\dot{\beta} \sin \beta - R\dot{\theta} \cos \theta = 0 \\ L\dot{\beta} \cos \beta - R\dot{\theta} \sin \theta = 0 \end{cases} \quad (38)$$

$T$ ,  $V$  and  $D$  can be calculated as

$$T = \frac{1}{2} M \dot{y}^2 + \frac{1}{2} m R^2 \dot{\theta}^2 = \frac{1}{2} M \dot{y}^2 + \frac{1}{2} m \dot{y}^2 \frac{\cos^2 \beta}{\cos^2(\theta - \beta)} \quad (49)$$

$$V = \frac{1}{2} k y^2 \quad (510)$$

$$D = \frac{1}{2} c \dot{y}^2 \quad (611)$$

Where:  $L$  - the length of the push rod;  $R$  - the radius of the seesaw;  $\beta$  - the angle between the push rod and the horizontal direction;  $\theta$  - the angle between the seesaw and the vertical direction;  $M$  - blade equivalent mass;  $m$  - virtual masses;  $k$  - blade equivalent stiffness;  $c$  - blade equivalent damping.

According to Eqs. (27) and Eqs. (38), the relevant terms in Eqs. (16) are obtained as

$$\begin{cases} \frac{d}{dt} \left( \frac{\partial T}{\partial \dot{y}} \right) = M \dot{y} + m \dot{y} \frac{\cos^2 \beta}{\cos^2(\theta - \beta)} + m \dot{y} \frac{d}{dt} \left[ \frac{\cos^2 \beta}{\cos^2(\theta - \beta)} \right] \\ \frac{\partial T}{\partial y} = \frac{1}{2} m \dot{y}^2 \frac{\partial}{\partial y} \left[ \frac{\cos^2 \beta}{\cos^2(\theta - \beta)} \right] \\ \frac{\partial V}{\partial y} = k y \\ \frac{\partial \Psi}{\partial \dot{y}} = c \dot{y} \\ Q(t) = F(t) \end{cases} \quad (712)$$

Then, the dynamic differential equation of test system is

$$\left\{ M + m \frac{\cos^2 \beta}{\cos^2(\theta - \beta)} \right\} \ddot{y} + c \dot{y} + k y + \frac{m \dot{y}^2 \cos \beta}{\cos^4(\theta - \beta)} \left[ \frac{\cos^2 \beta \sin(\theta - \beta)}{R} - \frac{\sin^2 \theta}{L} \right] = F(t) \quad (813)$$

**Where:** By comparison with Eqs. (4), it can be seen that the inertial force terms of two equations are same at the maximum amplitude of the blade.

$$\sin \theta = \frac{L+y}{R} - \frac{L(R\sqrt{-(y^2+2Ly-2LR)(y^2+2Ly+2LR)}+y^3+2L^3+4L^2y+3Ly^2)}{2R(L^3+2L^2y+LR^2+Ly^2)}$$

$$\cos \theta = \frac{L(L+y)[R\sqrt{-(y^2+2Ly-2LR)(y^2+2Ly+2LR)}+2L^3+y^3+3Ly^2+4L^2y]}{2R^2(L^3+2L^2y+LR^2+Ly^2)} - \frac{2L^2+2Ly-2^2+y^2}{2R^2}$$

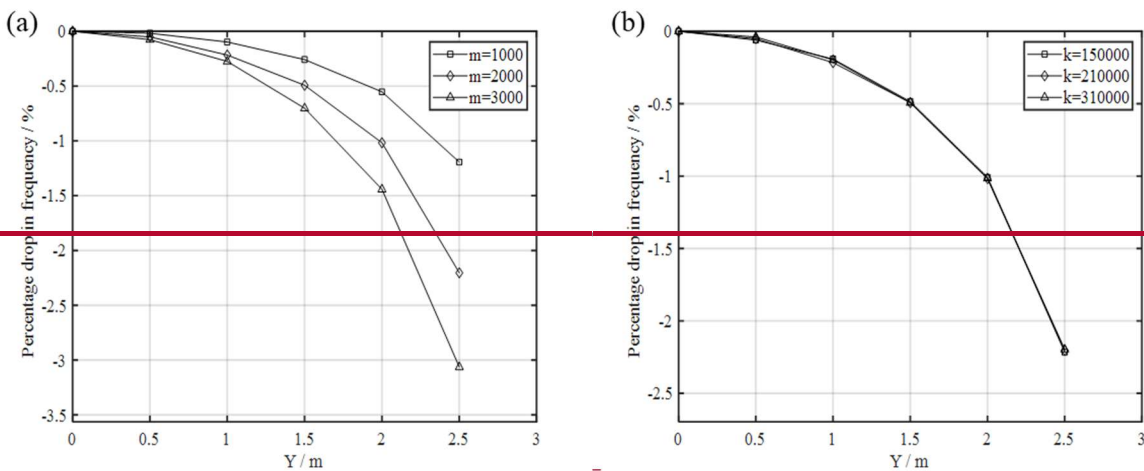
$$\sin \beta = \frac{2L^2+2Ly+^2}{2LR} - \frac{(L+y)[R\sqrt{-(y^2+2Ly-2LR)(y^2+2Ly+2LR)}+2L^3+y^3+3Ly^2+4L^2y]}{2R(L^3+2L^2y+LR^2+Ly^2)}$$

$$\cos \beta = \frac{R\sqrt{-(y^2+2Ly-2LR)(y^2+2Ly+2LR)}+2L^3+y^3+3Ly^2+4L^2y}{2(L^3+2L^2y+LR^2+Ly^2)}$$



According to Eqs. (813), it can be seen that rotation of virtual masses introduces nonlinear terms to the test system, and both the angle  $\theta$  and  $\beta$  are nonlinear functions of the blade response  $y$ . Due to the complexity of the dynamic equation, it is difficult to obtain the corresponding analytical expression. Therefore, the numerical analysis methods are used to solve the equation. A numerical simulation model based on the differential equation of the system motion is established in MATLAB SIMULINK, and the corresponding resonance frequency of the equivalent system can be obtained by setting different initial displacements. By modifying the value of the different parameter ( $m$ ,  $k$ ,  $R$ ), the influence of the parameter change on the resonance frequency of the test system can be obtained. As mentioned previously, the nonlinear factors that affect the characteristics of the test system mainly come from installation parameters (pushrod length and seesaw radius) and blade response. The design length of the push rod generally typically remains unchanged due to space limitations at the test site. However, the seesaw radius offers greater design flexibility. Thus, the primary focus is on evaluating the impact of the seesaw radius  $R$  and blade response  $y$  on the vibration characteristics of the blade. To illustrate this, the equivalent parameters of 80m blade are brought into the differential equation and numerically analyzed, and the influence of blade amplitude on the resonance frequency of the test system is investigated, as demonstrated in Fig. 4. numerical analysis is performed on the equivalent model of an 80m blade to examine the impact of blade amplitude on the resonance frequency of the testing system. This investigation is carried out by considering different virtual masses and radius of the seesaw, as demonstrated in Fig. 3.

Figure 3-4 (a) shows that the resonance frequency of the test system decreases nonlinearly with an increase in blade amplitude and virtual masses  $m$  further determines the rate of decrease in resonance frequency. The equivalent stiffness  $k$  has the ability to alter the natural frequency of the test system. However, it can be seen Fig. 3-4 (b) that  $k$  cannot change the rate of decrease in resonance frequency with other parameters unchanged, which indicates that the equivalent stiffness is not a nonlinear factor affecting the vibration characteristics of the testing system. Fig. 4 (c) shows that the increase of  $M$  will delay the decline rate of the natural frequency of the system, because the proportion of the virtual masses in the inertia force term decreases. It can be seen from Fig. 4 (d) Fig. 3 (a) shows that the radius of the seesaw will also affect the nonlinear amplitude-frequency characteristics of the test system and the rate of decrease in resonance frequency.



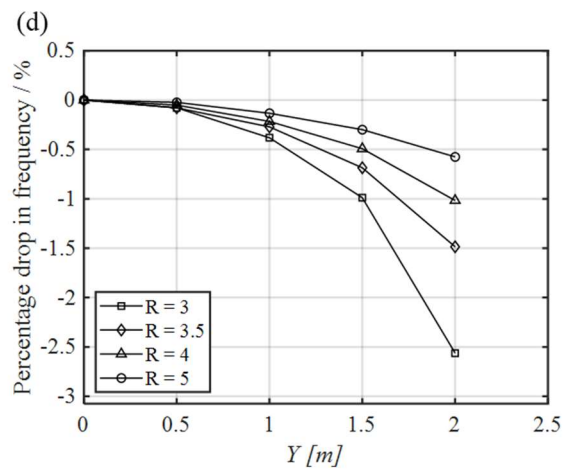
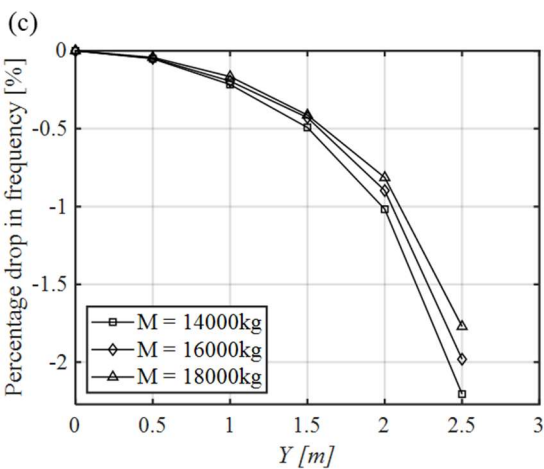
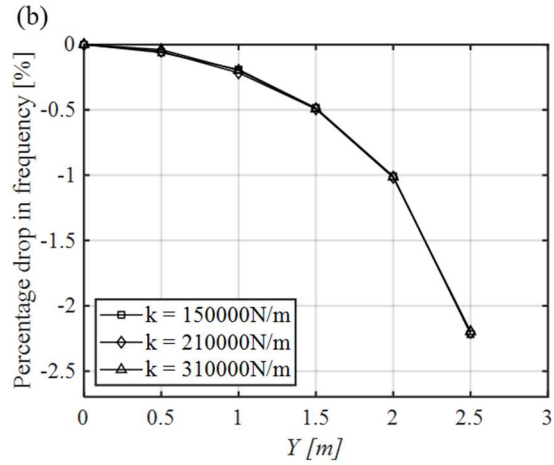
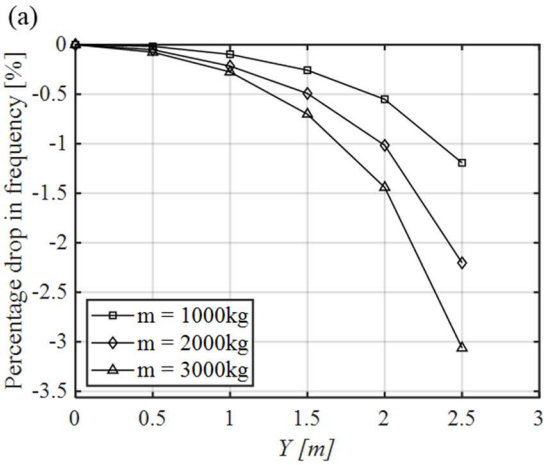
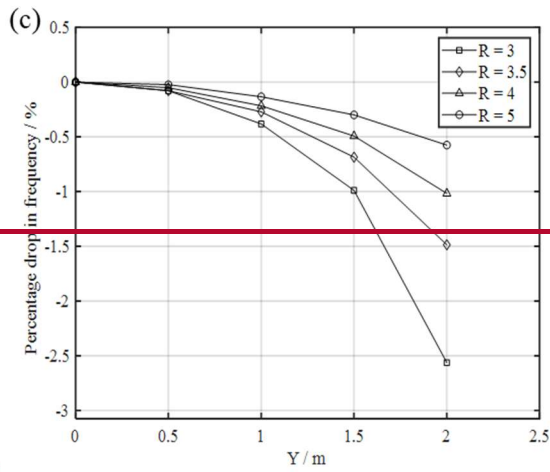


Figure 34: The relationship between resonance frequency and amplitude of the blade at different parameters: (a)  $M = 14000\text{kg}$ ;  $k = 210000\text{N/m}$ ;  $L = 4\text{m}$ ;  $R = 4\text{m}$  (b)  $M = 14000\text{kg}$ ;  $m = 2000\text{kg}$ ;  $L = 4\text{m}$ ;  $R = 4\text{m}$  (c)  $k = 210000\text{N/m}$ ;  $m = 2000\text{kg}$ ;  $L = 4\text{m}$ ;  $R = 4\text{m}$  (d)  $M = 14000\text{kg}$ ;  $k = 210000\text{N/m}$ ;  $m = 2000\text{kg}$ ;  $L = 4$ .

### 2.2.3 Analysis of amplitude-frequency characteristics of the model

As previously mentioned, both virtual mass and traditional additional masses adjust the load distribution of the measured blade by changing the modal characteristics of the blade through the inertial force originated from the blade movement. However, due to the motion of the virtual masses mechanism, a distinct inertial force from that of traditional additional masses, which contributes to the nonlinearity of the test system. The dynamic differential equations of the blade-virtual masses test system, established through the Lagrange method, are highly complex and can only be resolved numerically to derive the correlations among the relevant parameters and the resonance frequency of the test system. To quantitatively further analyze



the nonlinear amplitude-frequency characteristics of the test system, it is necessary to ~~construct~~ create a theoretical model of the test system based on nonlinear dynamics (Liu et al., 2001). According to linear vibration theory (Liu et al., 2001), the factors that primarily influence the inherent characteristics of a linear system are the inertial force term and the elastic force term. In fact, the inherent characteristics of the blade-virtual masses test system are primarily determined by the inertial force term associated with the introduction of virtual ~~mass~~ masses and the response of the blade. Thus, the weakly nonlinear dynamic equation of the blade-virtual ~~mass~~ masses test system in Eqs. (13) Fig-2 can be approximated as:

$$(M + m)f(y)\ddot{y} + c\dot{y} + ky = F_0 \cos(\omega t + \theta) \quad \text{---(914)}$$

Where:  $f(y) = 1 + \varepsilon_1 y + \varepsilon_2 y^2 + \varepsilon_3 y^3 + \varepsilon_4 y^4$ ;  $c = 2\zeta(M + m)\omega_n$ ;  $k = (M + m)\omega_n^2$ ;  $F_0 = Bk$ ;  $\varepsilon_1, \varepsilon_2, \varepsilon_3, \varepsilon_4$  - Small parameters related to  $M, m, L$  and  $R$ ;  $\zeta$  - Damping ratio;  $\omega_n$  - Natural frequency;  $\omega$  - Excitation frequency;  $\theta$  - Phase difference between steady-state response and excitation.

Ignoring the small parameters, Eqs. (914) is transformed into the vibration equation of a linear system. This means that the linear system is derived from the original nonlinear system. To quantitatively analyze the modal characteristics of the test system, the approximate analytical method can be employed by considering the nonlinear factor as a perturbation to the linear system, yielding an approximate analytical solution for the nonlinear system. Among various approximate analytical methods, the harmonic balance method is particularly notable due to its clear conceptual foundation. It expands both the excitation term and the solution of the equation into a Fourier series. From a physical perspective, the coefficients of the harmonic terms of the same order at both ends of the dynamic equation must be equal to maintain a balance between the excitation and inertia forces. When the condition of the test system is determined, the value of the small parameter in Eqs. (914) is also determined.

For the blade-virtual masses testing system, it is assumed that its steady-state response is still periodic, but the resonance frequency is different from the natural frequency of the derived system. The basic solution is expanded into the Fourier series of the excitation frequency and the fundamental component is retained. The response of the system as Eq. (4015) indicates.

$$y(t) = Y_0 \cos(\omega t) \quad \text{---(4015)}$$

Where:  $Y_0$  - Amplitude of blade steady-state response.

By substituting Eq. (4015) into Eq. (914) and applying the triangle transform and harmonic balance to eliminate the phase difference  $\theta$  to achieve the relationship between the amplitude and frequency of the test system, as Eq. (4116) indicates.

$$\left[1 - s^2 \left(1 + \frac{3}{4}\varepsilon_2 Y_0^2 + \frac{10}{16}\varepsilon_4 Y_0^4\right)\right]^2 + (2\zeta s)^2 = \left(\frac{B}{Y_0}\right)^2 \quad \text{---(4116)}$$

Where:  $s = \omega/\omega_n$ .

According to Eq. (4116), The amplitude-frequency and phase-frequency characteristics of the nonlinear system can be obtained, as Eq. (4217) indicates.

$$\begin{cases} \frac{Y_0}{B} = \frac{1}{\sqrt{\left[1 - s^2 \left(1 + \frac{3}{4}\varepsilon_2 Y_0^2 + \frac{10}{16}\varepsilon_4 Y_0^4\right)\right]^2 + (2\zeta s)^2}} \\ \theta = \arctan \left[ \frac{2\zeta s}{1 - s^2 \left(1 + \frac{3}{4}\varepsilon_2 Y_0^2 + \frac{10}{16}\varepsilon_4 Y_0^4\right)} \right] \end{cases} \quad \text{---(4217)}$$

When  $\varepsilon_2 = \varepsilon_4 = 0$ , Eq. (4217) describes the amplitude-frequency characteristics of a linear system, as shown in Fig. 45. When the small parameters are non-zero, the amplitude-frequency characteristic curve of the nonlinear system is depicted in Fig. 56. Similar to forced vibrations in linear systems, nonlinear systems also exhibit similar amplitude-frequency characteristic curves. However, the backbone of the support curve clusters is not straight but inclined. This backbone curve represents the variation of the free vibration frequency of the nonlinear system with respect to the amplitude when there is no external excitation (Liu et al., 2001). By setting  $B = 1$  and  $\zeta = 0$  in Eq. (4116), the equation for this backbone curve can be obtained, as Eq. (4318) indicates.

$$\omega^2 = \frac{\omega_n^2}{\left(1 + \frac{3}{4}\varepsilon_2 Y_0^2 + \frac{10}{16}\varepsilon_4 Y_0^4\right)} \quad \text{---(4318)}$$

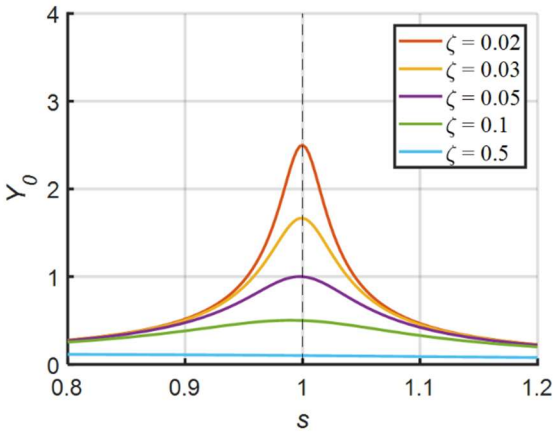
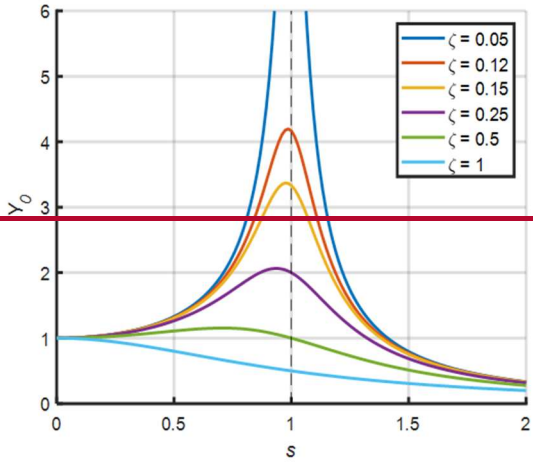
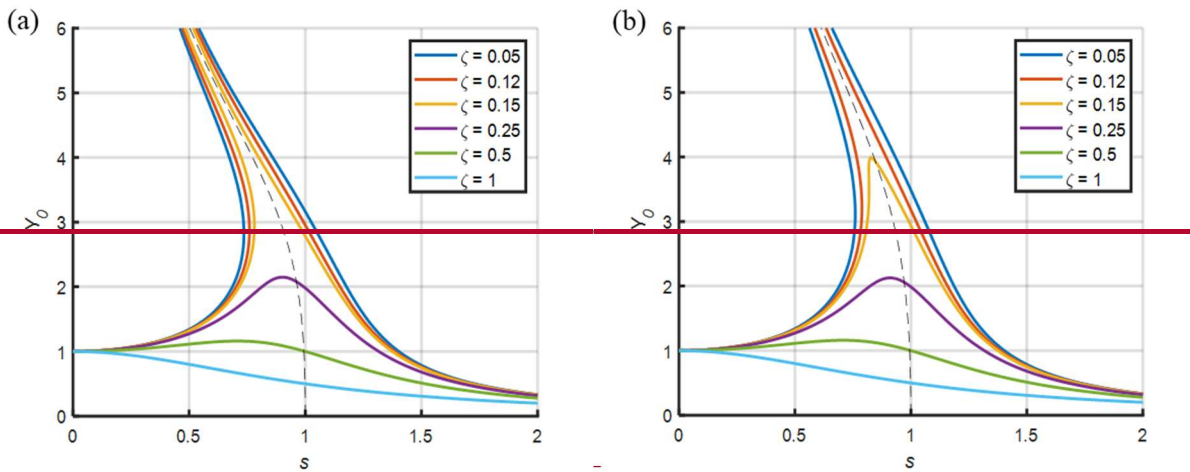


Figure 45: Amplitude-frequency characteristic curve of a linear system

Eq. (4318) shows that the resonance frequency of the blade-virtual masses test system decreases with the increase of the amplitude of the blade and there exists the nonlinear relationship between the square of the frequency ratio and the amplitude. Figure 5-6 shows that the small parameters in the inertial force term will affect the frequency of free vibration. As these parameters decrease, the amplitude-frequency characteristic curve of a nonlinear system approaches that of a linear system, and the backbone curve approaches a value close to 1.



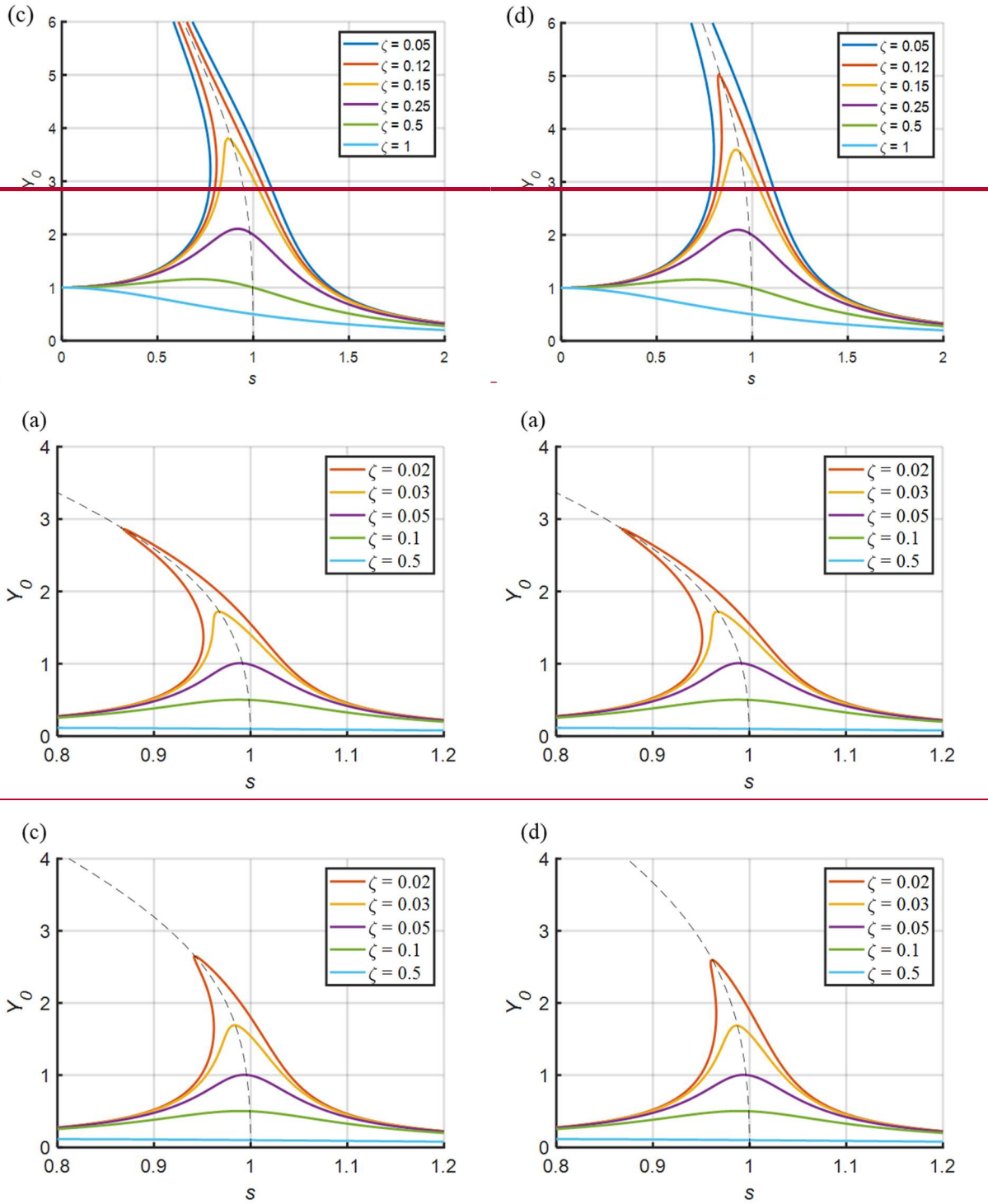


Figure 56: Amplitude-frequency characteristic and the backbone (represented by the black dashed line) of the blade-virtual masses testing system: (a)  $B = 0.1, \frac{3}{4}\varepsilon_2 = 0.01, \frac{10}{16}\varepsilon_4 = 0.002$  (b)  $B = 0.1, \frac{3}{4}\varepsilon_2 = 0.01, \frac{10}{16}\varepsilon_4 = 0.001$  (c)  $B = 0.1, \frac{3}{4}\varepsilon_2 = 0.005, \frac{10}{16}\varepsilon_4 = 0.001$  (d)  $B = 0.1, \frac{3}{4}\varepsilon_2 = 0.005, \frac{10}{16}\varepsilon_4 = 0.0005$ .

Figure 6 shows the influence of different small parameters on the amplitude-frequency characteristics of the system. In fact, specific small parameter values mean specific working conditions, that is, when the virtual mass related parameters (such as  $L, R, m$ ) are determined, the amplitude-frequency characteristics of the system will also be determined. Therefore, as long as the setups are determined, the dynamic characteristics of the test system will be determined, whether it is a single axis test or a biaxial test.

In addition, the amplitude hopping phenomenon, also known as dynamic bifurcation, also appears in Figure 6. In fact, there is no obvious dynamic bifurcation phenomenon in the fatigue test, because the nonlinearity of the system is

weak, and the amplitude of the blade is limited by the size of the mechanism. Moreover, when the influence of blade amplitude on the resonance frequency of the system is discussed in the following paper, more attention is paid to the backbone curve in the shape of the black dotted line in Fig. 6.

### 3 Dynamic simulation analysis

To validate the nonlinear characteristics of the blade-virtual ~~massmasses~~ test system that has been established, it is necessary to utilize multi-body dynamics simulation software ADAMS to create a realistic blade model for analysis. Based on the sectional properties and tuning masses of the blade, ~~ADAMS motion analysis software~~ can be employed for modeling and analyzing the blade-virtual masses system. ~~ADAMS The simulation software~~ can perform modal analysis and transient sweep frequency harmonic analysis to obtain the changing characteristic of the testing system under various operating conditions. As the foundation for other dynamics analysis, modal analysis is used to determine the modal characteristics of structures. Regarding the weakness of modal analysis function in the software, which cannot consider the effects of the response on the modal characteristics of the system, it is necessary to take further transient sweep-frequency analysis to obtain the resonance characteristics of the system.

#### 3.1 Simulation ~~Modeling~~Modelling

To verify that the simplified equivalent theoretical model can reflect the characteristics of actual test system, the simulation model is established in software. Generally, only the cross-section stiffness (flap-wise and edge-wise) and linear density are considered in the simulation model (Post et al., 2016), because the torsional natural frequency is much higher than the natural frequency in the direction of flap-wise and edge-wise, it is difficult to stimulate large torsional deformation. The root of the blade was set as a fixed constraint to simulate the cantilever beam condition similar to when the blade is mounted on the test rig. The equivalent damping ratio of the blade changes during vibration, resulting in a change in the resonance frequency of the test system (Lee., 2018; Liu et al., 2019). In order to accurately assess the influence of virtual ~~massmasses~~ on the characteristics of the testing system, aerodynamic damping is not considered in the simulation model. The blade model was built in the simulation software based on the parameters mentioned above, as shown in Fig. 67(a).

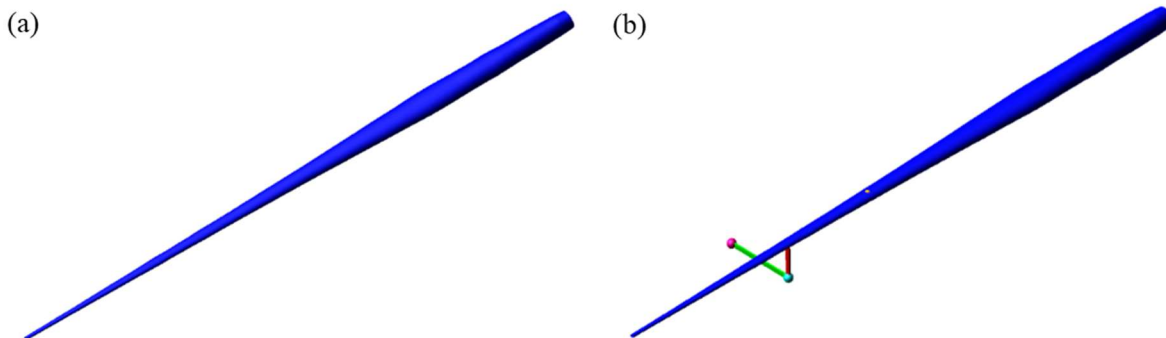


**Figure 67: Dynamics simulation model of test system: (a) The blade simulation model (b) The blade-virtual masses simulation model(flap-wise)**

#### 3.2 Model validity verification

To ensure the applicability and rationality of the model, modal analysis is carried out and compared with the transfer-matrix method (TMM) and the test data, ~~taking the calculation of the flap wise direction as an example,~~ as shown in Table 1. The transfer matrix method is an approximate theoretical method used to calculate the natural frequencies and modes of systems with chain structures. The transfer matrix method separates the structure with inertia and elasticity and obtains the relationship between the discrete elements. The natural frequencies and modes of the systems can be solved according to the boundary conditions. The transfer matrix method belongs to the physical discrete method of continuous system, which is suitable for numerical solution of blade model. The blades in Table 1 were all subjected to actual modal tests, and the obtained

frequency data are obtained from the frequency domain analysis of actual test data. The actual blade modal test was carried out by hammer method. It can be seen that the simulation model of the test system has good applicability exhibits a high level of accuracy, with an error in the modal frequency of less than 4%.

**Table1. Blade modal analysis in flap-wise direction Comparison of natural frequencies calculated by various methods**

Flap-wise			84m		94m	
Method	1st modal frequency [Hz]	Error [%]	1st modal frequency [Hz]	Error [%]		
Test	0.394	-	0.365	-		
TMM	0.397	+0.7	0.349	-4.38		
Simulation	0.404	+2.54	0.377	+3.29		

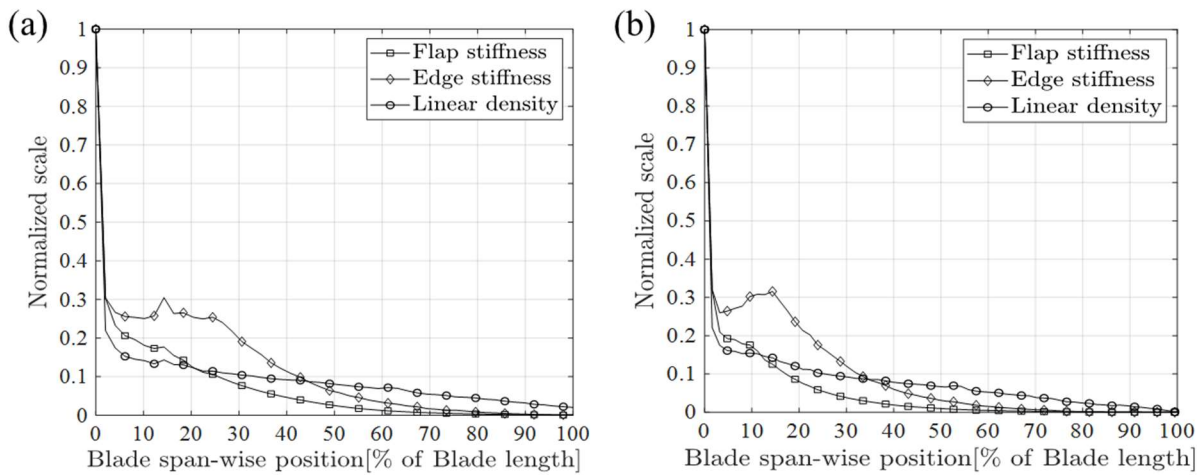
<u>Edge-wise</u>			<u>84m</u>		<u>94m</u>	
<u>Method</u>	<u>1st modal frequency [Hz]</u>	<u>Error [%]</u>	<u>1st modal frequency [Hz]</u>	<u>Error [%]</u>		
<u>Test</u>	<u>0.590</u>	<u>-</u>	<u>0.571</u>	<u>-</u>		
<u>TMM</u>	<u>0.604</u>	<u>+2.37</u>	<u>0.561</u>	<u>-1.75</u>		
<u>Simulation</u>	<u>0.610</u>	<u>+3.34</u>	<u>0.589</u>	<u>+3.15</u>		

### 3.3 Simulation setup

With the purpose of demonstrating the nonlinear effects of rotating virtual masses on the testing system, it is necessary to add virtual masses based on the blade model, as shown in Fig.67(b). The values of the additional masses are shown in Table 2 and the section properties of the blades are shown in Fig. 78. The position and values of the tuning additional masses are provided by the blade manufacturer. Virtual mass masses elements are added at 62% and 49% of the 84m blade length in the flap-wise and edge-wise directions respectively. Similarly, virtual mass masses elements are added at 63% and 52% of the 94m blade length in the flap-wise and edge-wise directions respectively (masses marked in black italics in Table 2). The constraints for the seesaw, push rod, and virtual masses are set according to Fig. 1, where the rotation center of the seesaw is set as the revolute pair and the seesaw and push rod are set as the rigid light rod. To evaluate and verify the effects of virtual masses installation parameters and blade response on the vibration characteristics of the testing system, not only the effects of radius of the seesaw and blade response on the resonance frequency, but also the effects of radius of the seesaw on the load distribution of the blade with similar amplitude are analyzed through simulation.

**Table2. Blade additional masses of 84m and 94m blade**

84m			94m		
Location	Flap-wise masses [kg]	Edge-wise masses [kg]	Location	Flap-wise masses [kg]	Edge-wise masses [kg]
26%		2835	42%	3000	3000
36%		3147	52%		<b>4075</b>
49%	6120	<b>4075</b>	63%	<b>1116</b>	
62%	<b>1117</b>				



356  
357 **Figure 78: Section properties of the blade: (a) 84m blade (b) 94m blade**

358 ~~As the foundation for other dynamics analysis, modal analysis is used to determine the modal characteristics of structures.~~  
 359 ~~Regarding the weakness of modal analysis function in the software, which cannot consider the effects of the response on the~~  
 360 ~~modal characteristics of the system, it is necessary to take further sweep frequency analysis to obtain the resonance~~  
 361 ~~characteristics of the system. The sweep frequency analysis is to apply a series of harmonic excitation with different~~  
 362 ~~frequencies to the system to analyze its response spectrum.~~

363 **4 Results**

364 According to the backbone in the amplitude-frequency characteristic curve of the blade-virtual masses test system, when the  
 365 operation condition determined, the square of the resonance frequency and the blade amplitude satisfy the relationship in Eqs.  
 366 (4318). Thus, correlated simulation results are fitted using relevant functions to verify the relationship.

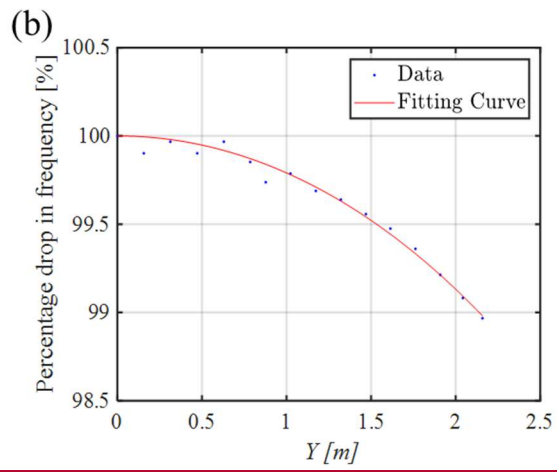
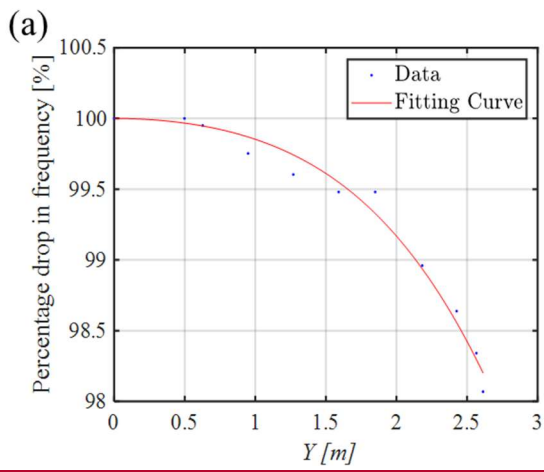
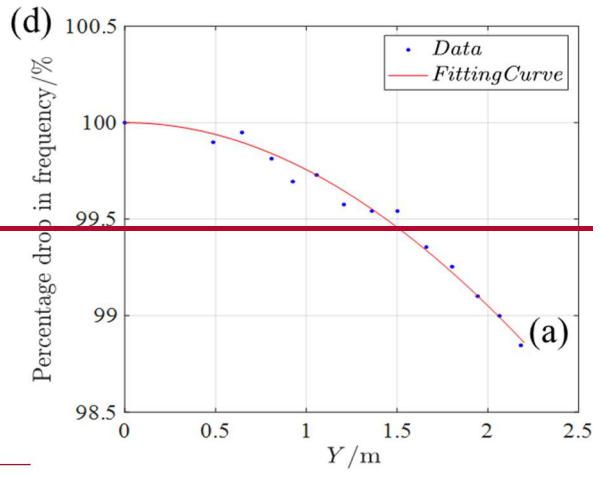
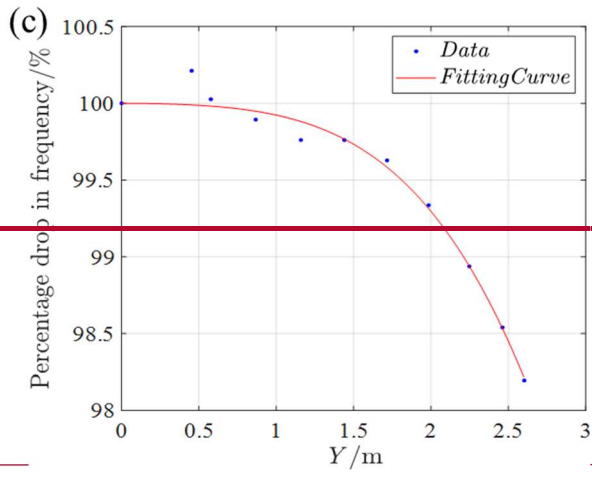
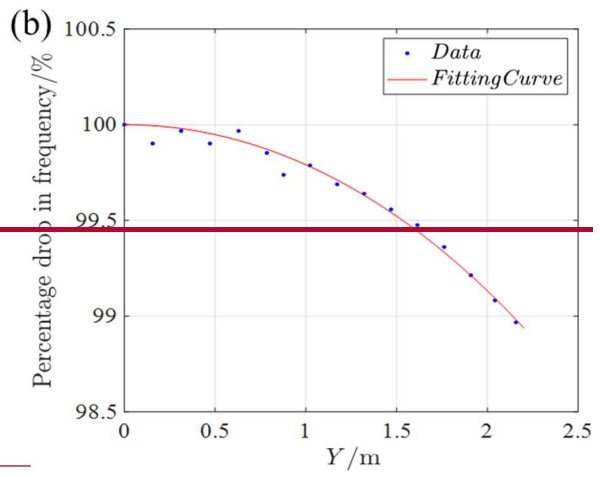
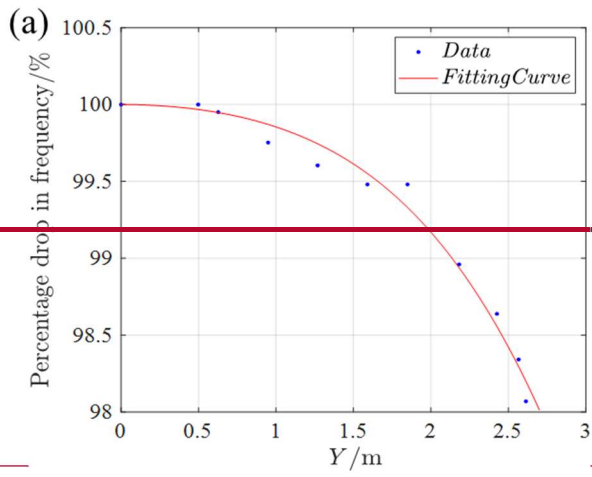
367 **4.1 Effects of amplitude on resonance frequency**

368 **4.1.1 Effects of blade amplitude on resonance frequency**

369 Set  $R = 4\text{m}$  and  $L = 4\text{m}$  and investigate the variation of the resonance frequency of test system under different amplitudes.  
 370 Sweep-frequency analysis is performed on the 84m and 94m blades in flap-wise and edge-wise directions respectively to obtain  
 371 the resonance frequencies of the test system under different steady-state amplitudes while the results are fitted according to  
 372 Eqs. (4318), as shown in Fig. 89. ~~In addition, the degree of fit is expressed by goodness of fit  $R^2$ . The sweep frequency range~~  
 373 ~~is defined as a bandwidth of 0.02Hz near the first natural frequency in the flap-wise or edge-wise direction, with an~~  
 374 ~~action time of 1E4s and a resolution of 2e-6 Hz/sec. The frequency spectrum of the displacement of the exciting point~~  
 375 ~~of the blade under the sweeping excitation is analyzed, and the frequency corresponding to the peak point is the resonance~~  
 376 ~~frequency. The mechanism might reach the geometric limit of the push-rod parallel to the seesaw, so the limit~~  
 377 ~~requirements of the mechanism need to be considered.~~

378 When amplitude of the blade is small, the percentage drop in resonance frequency is small. When amplitude of the blade  
 379 is large, the resonance frequency presents nonlinear ~~rapid decline~~ ~~faster~~. When the blade amplitude in flap-wise direction  
 380 reaches 2.6m, the resonance frequency of the 84m and 94m blades decreases by approximately 2.0%; When the blade  
 381 amplitude in edge-wise direction reaches 2.2m, the resonance frequency of the 84m and 94m blades decreases by  
 382 approximately 1.1%. ~~Due to the limitation of resonance frequency extraction precision in sweep frequency analysis, the~~  
 383 ~~fitting degree of data is affected. However, it is still acceptable at the large amplitude of the blade. Combined with the~~  
 384 ~~actual test requirements, we should pay more attention to the conditions of large amplitude.~~





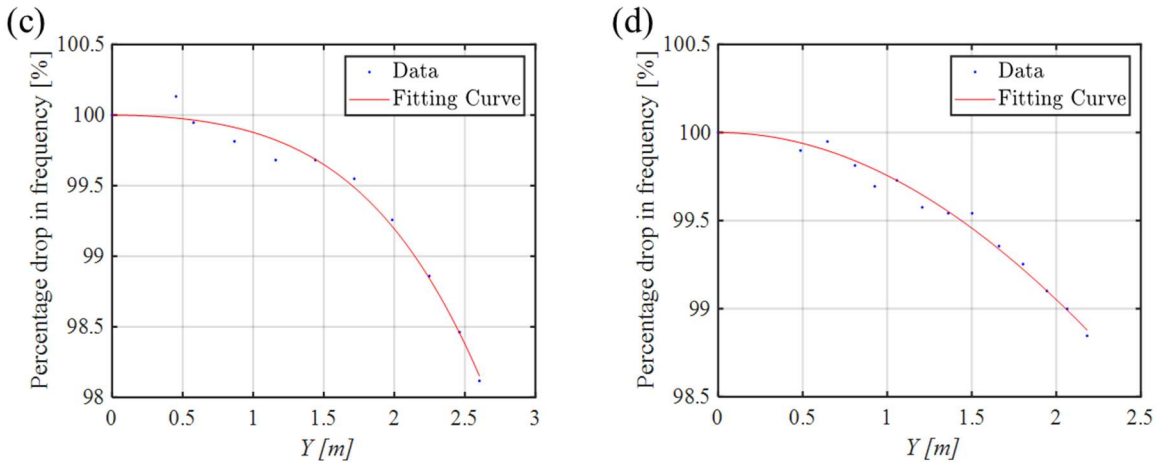


**Figure 89:** Relationship between amplitude and percentage drop in resonance frequency: (a) 84m blade in flap-wise direction ( $R^2 = 0.9814$ ); (b) 84m blade in edge-wise direction ( $R^2 = 0.9829$ ); (c) 94m blade in flap-wise direction ( $R^2 = 0.9861$ ); (d) 94m blade in edge-wise direction ( $R^2 = 0.9831$ )

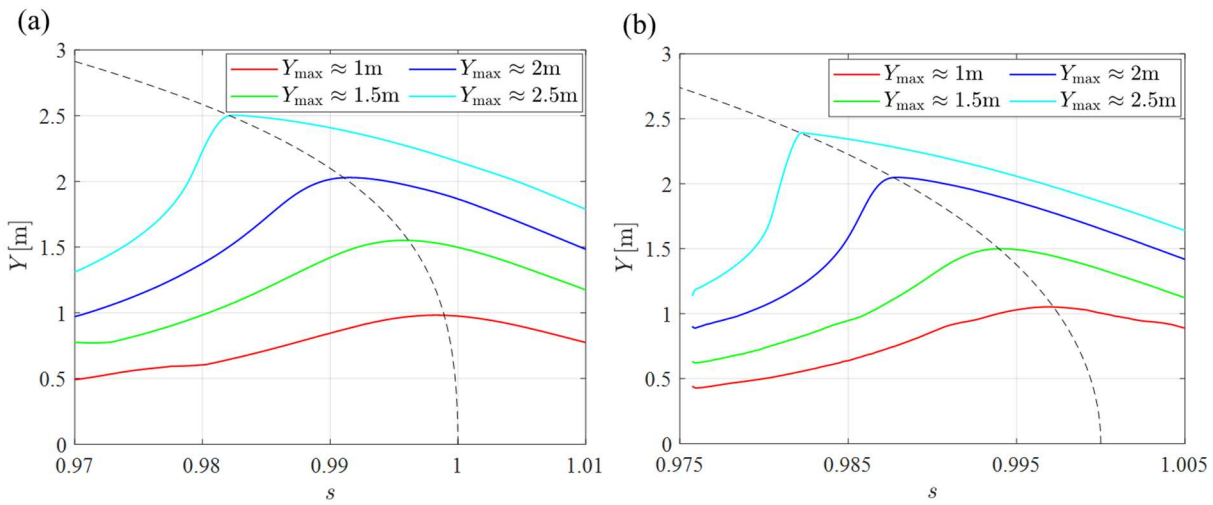


**Figure 10:** The sweep spectrum of the blade under different target amplitudes

Taking 94m blade as an example, the sweep spectrum of the blade under different target amplitudes is shown in Fig. 10. It can be seen from Fig.10 that different excitation frequencies cause different blade responses. The resonance frequency of the system decreases with the increase of the maximum amplitude of the blade. This also verifies the applicability of the approximate amplitude-frequency properties obtained by the theory (Fig. 6 has a backbone curve similar to Fig. 10).

#### 4.1.2 Effects of radius of the seesaw on resonance frequency and load distribution

Considering the actual experimental-test setup, the blade amplitude in flap-wise direction is set to be about  $Y=2\text{m}$  and the length of the push rod is  $L=4\text{m}$ ; the blade amplitude in edge-wise direction is about  $Y=1\text{m}$  and the length of the push rod is  $L=4\text{m}$ . The sweep-frequency analysis of the 84m and 94m blades in flap-wise and edge-wise directions is carried out respectively to obtain the resonance frequency of the test system. According to Eqs. (1318), appropriate function (Eqs. (1419)) is selected to fit the results, as shown in Fig. 911. Eqs. (19) is a function selected according to the degree of best fit. Considering equations (1318) and (1419), the small parameters encompass the influence of radius of the seesaw, which can be approximated by an exponential function. A larger radius of the seesaw results in a smaller decrease in the resonance frequency. Conversely, when the rotation radius of the seesaw is small, the resonance frequency experiences a rapid and nonlinear decrease. With  $R = 3\text{m}$ , the drop in the resonance frequency of the 84m and 94m blades is approximately 1.6% in the flap-wise direction. Likewise, with  $R = 2\text{m}$ , the drop in the resonance frequency is approximately 1.1% in the edge-wise direction.

409

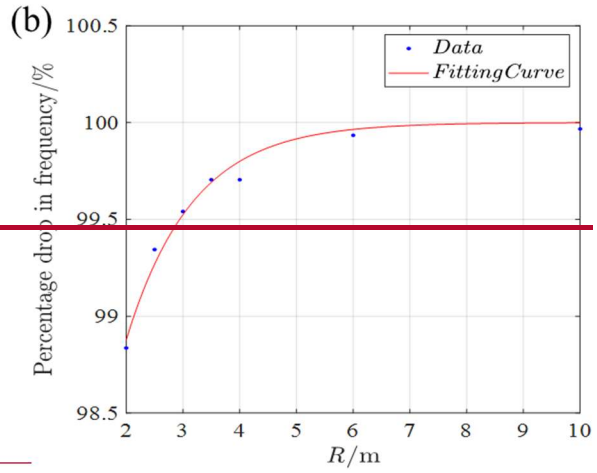
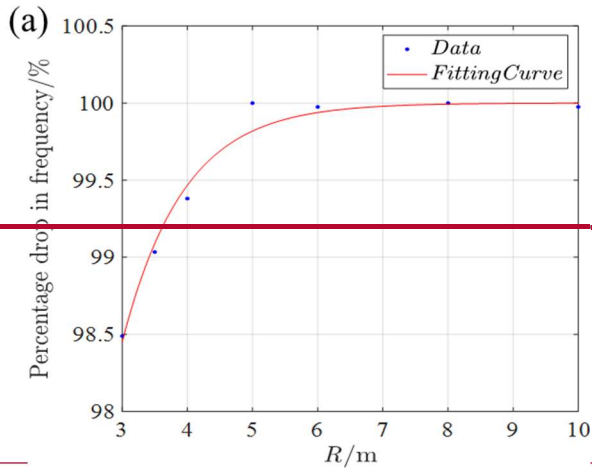
$$\omega^2 = \frac{\omega_n^2}{(1+ae^{-bR})}$$

\_(1419)

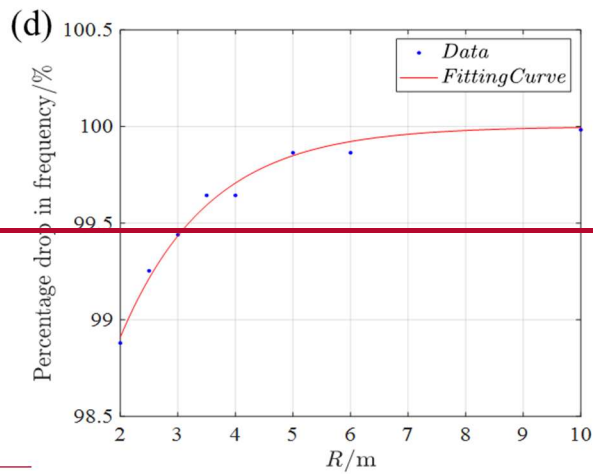
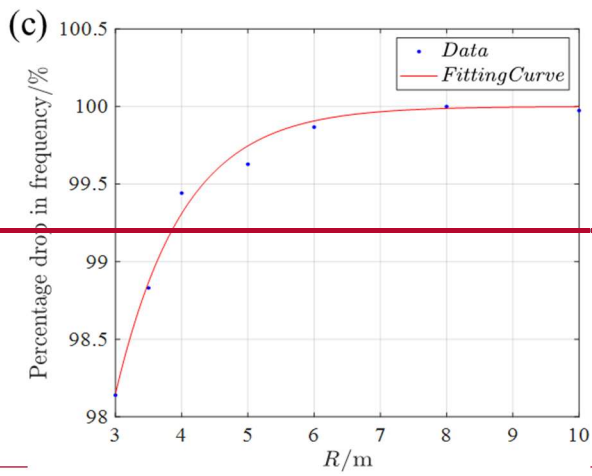
410

Where:  $a$  ,  $b$  - parameters in exponential function.

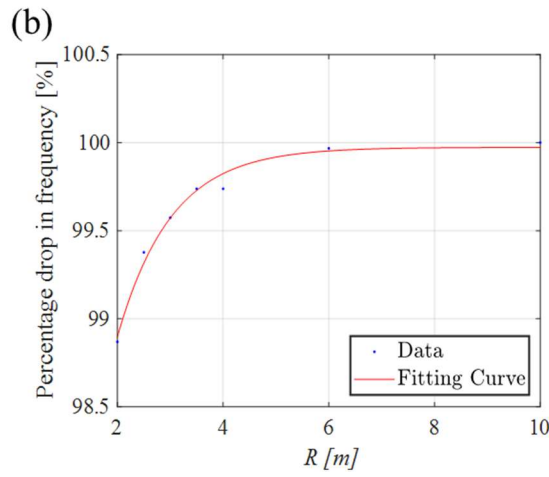
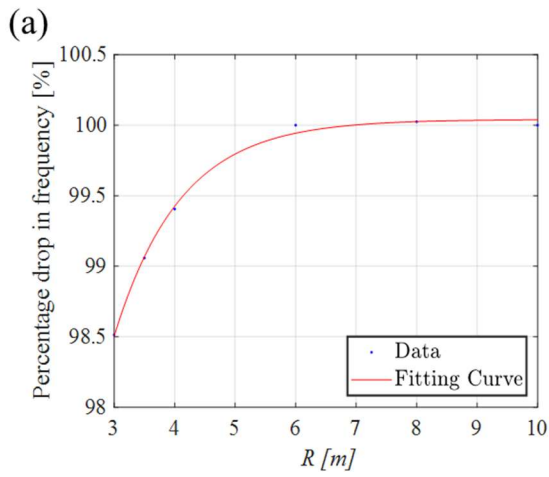
411

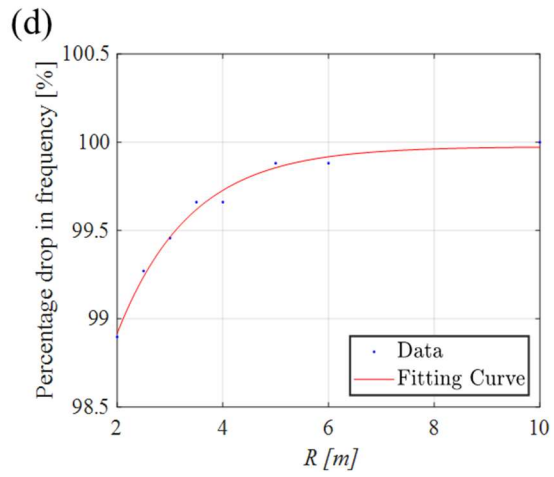
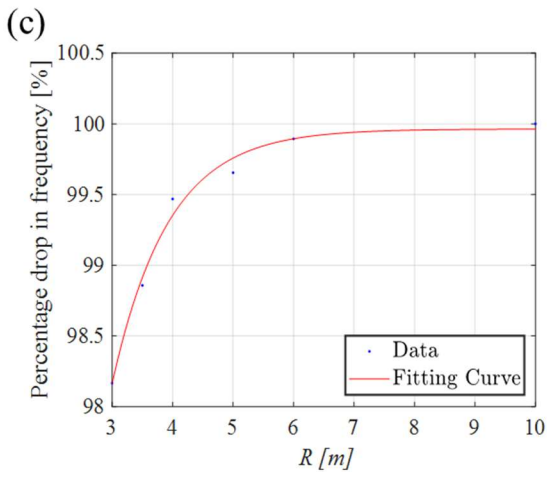


412

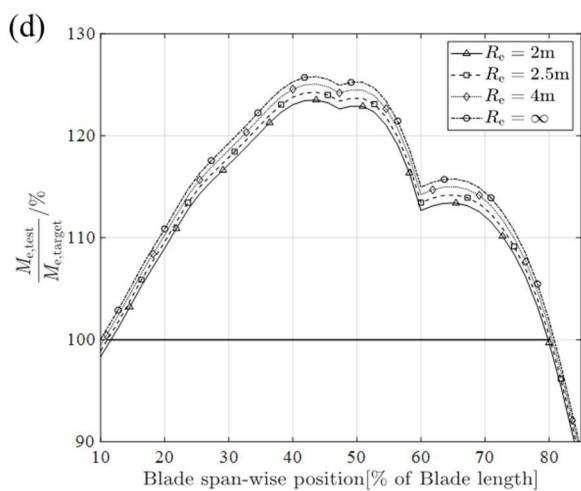
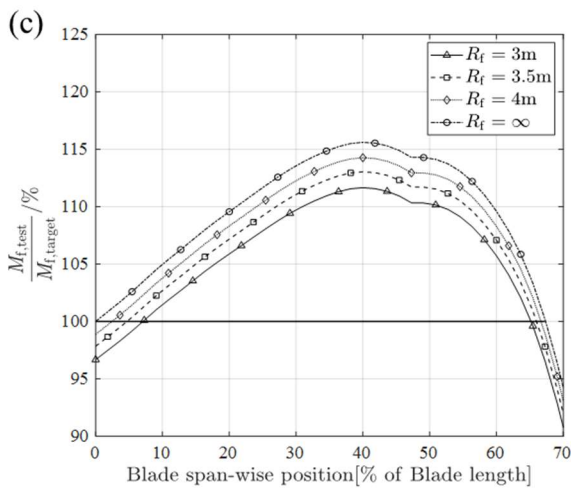
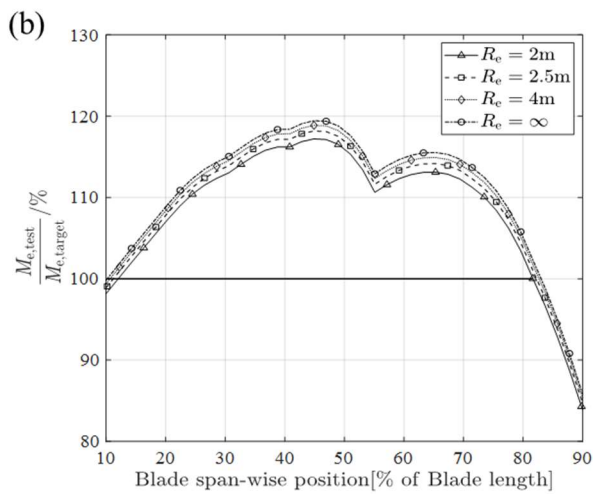
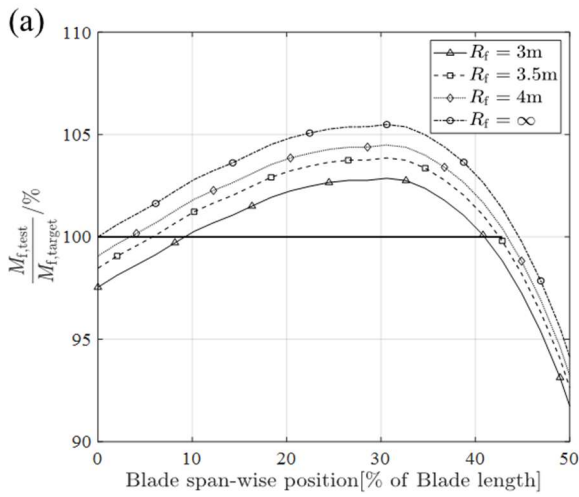


413





414  
415 **Figure 911:** Relationship between radius of the seesaw and percentage drop in resonance frequency: (a) 84m blade in flap-wise  
416 direction ( $R^2 = 0.9973$ ); (b) 84m blade in edge-wise direction ( $R^2 = 0.9786$ ); (c) 94m blade in flap-wise direction ( $R^2 =$   
417  $0.9884$ ); (d) 94m blade in edge-wise direction ( $R^2 = 0.9890$ )



419  
420 **Figure 1012:** Relationship between radius of the seesaw and blade load distribution: (a) 84m blade in flap-wise direction (b) 84m  
421 blade in edge-wise direction (c) 94m blade in flap-wise direction (d) 94m blade in edge-wise direction

422 In order to compare the influence of nonlinearity on the blade load distribution, the blade bending moment  
423 distribution can be calculated by using constant displacement of the exciting point and inertial load provided by virtual  
424 mass motion. The excitation position is the same as installation position of the virtual masses closest to the tip of the

blade, and the specific values are shown in Table 2. The excitation frequency is the resonance frequency of the respective vibration direction, which is obtained by the sweep frequency analysis.

The radius of the seesaw influences the characteristics of the testing system and alters the distribution of blade loads, as shown in Fig. 1012. In the case of  $R = \infty$ , the virtual masses shift from rotation to translation in the uniaxial test, effectively simulating additional masses that are directly fixed onto the blade. As  $R$  decreases, the amplitude of blade loads reduces rapidly. Consequently, there is an approximate 3% decrease in the overall load distribution in the flap-wise direction, resulting in a reduction in the area of interest the area which is actually fully tested will be reduced. Given the roughly similar amplitudes, lower resonance frequencies frequency results in reduced inertial loads on the blade. Therefore, compensatory measures such as increasing the excitation level are necessary during the actual test. However, this requires more powerful excitation equipment.

#### 4.3.2 Effects of virtual masses on biaxial test

In Section 4.1, only the effect of virtual masses on the uniaxial test is considered, which can intuitively see the influence of independent parameters on the vibration characteristics of the test system and blade load distribution from the uniaxial model. However, it is not enough to consider only the uniaxial vibration, but also the effect of virtual masses on the system in the biaxial vibration. Virtual masses will affect the resonance characteristics and load distribution in both flap-wise and edge-wise directions. In the biaxial fatigue test, the blade has a complex spatial trajectory, and the test system will be affected by multiple nonlinear parameters at the same time. To find the resonance frequency of the two directions, it is necessary to use the simulation software for iterative calculation. the coupling of vibrations in both directions further exacerbates the nonlinearity of the test system.

Taking 94m blade as an example, virtual masses are applied in both flap-wise and edge-wise directions. Modal analysis and frequency sweep analysis are used to obtain the frequencies at which specific excitations are applied to the test system. Combined with the actual working conditions, the flap amplitude at 63% position of the blade is about 2m, and the edge amplitude at 52% position of the blade is about 1m. The resonance frequencies under different conditions are The parameters are shown in Table 3, with  $R = 4m$  and  $L = 4m$ . In fact, the oscillations in flap-wise and edge-wise direction must not be evaluated separately as they influence each other, so the resonance frequency of the blade in each direction is obtained by sweeping frequency iteration. The spatial coupling trajectory of the blade can be obtained, as shown in Fig. 11. The results show that the resonance frequencies decrease compared to uniaxial test, especially in the flap wise direction, due to the influence of the virtual masses in both vibration directions. This is because the flap wise direction has a larger amplitude, and the inertial forces generated by the virtual masses in the edge wise direction produce more significant inertial component forces to the flap wise direction. Additionally, if do not consider the influence of the blade's structural twist. It can be seen from Fig.11 that the envelope of the blade's spatial trajectory is not a regular quadrilateral, which poses new challenges for adjusting the biaxial load distribution and damage assessment. Fig. 12 shows the spatial trajectory of the blade under the action of different virtual mass mechanisms. The results show three main characteristics: 1) Under the same exciting force, the resonance frequency of the two directions in the biaxial test is lower than that of the uniaxial test, which indicates that the virtual masses affect both vibration directions. 2) Compared with the ideal working condition, the virtual masses will deform the space trajectory of the blade (even considering the structural torsion of the blade), which is determined by the motion characteristics of mechanism. In addition, the deformation of the trajectory may bring higher requirements for the actual damage assessment of the blade. 3) Under the same exciting force, the difference between the average flap amplitude of the blade using the rotating virtual mass mechanism and the average flap amplitude under the ideal condition is 9%, and the difference between the average edge amplitude and the average edge amplitude under the ideal condition is nearly 11%, as shown in Table 4. Combined with the effect of reduced resonance frequency and amplitude, the biaxial load distribution level of the blade will be further reduced compared with the uniaxial test, which means that more energy input is required.

Table3. Biaxial excitation parameters of 94m

Virtual masses and exciting point	Modal analysis	Sweep frequency analysis
-----------------------------------	----------------	--------------------------



	Position [% of Blade length]	Force [N]	Natural frequency [Hz]	Amplitude at 63% position [m]	Resonance frequency [Hz]	Amplitude at 63% position [m]
Flap-wise	63%	3800	0.377	1.685	0.372	1.893
Edge-wise	52%	7000	0.589	1.292	0.586	1.402

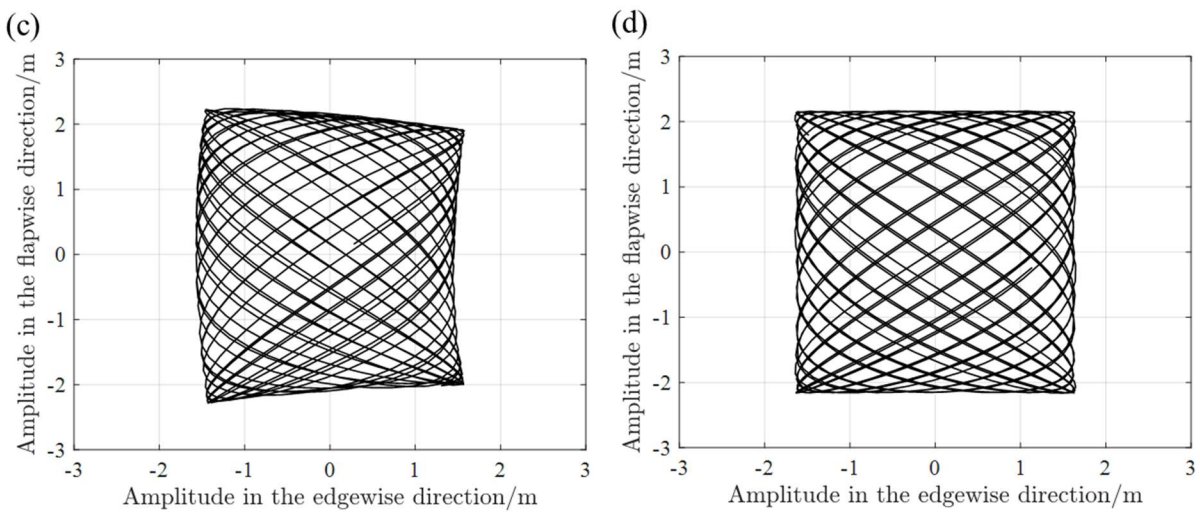
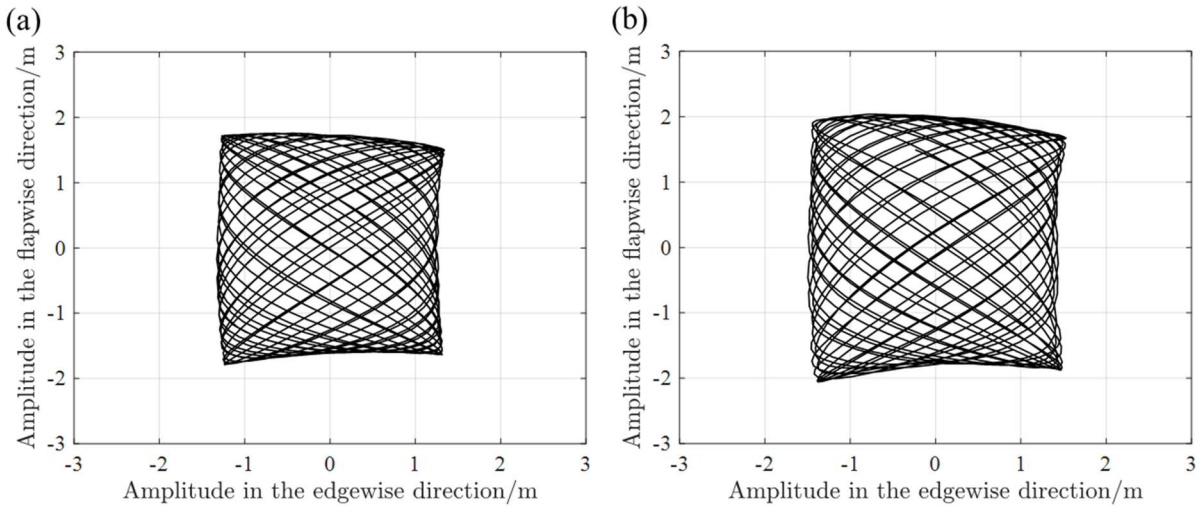
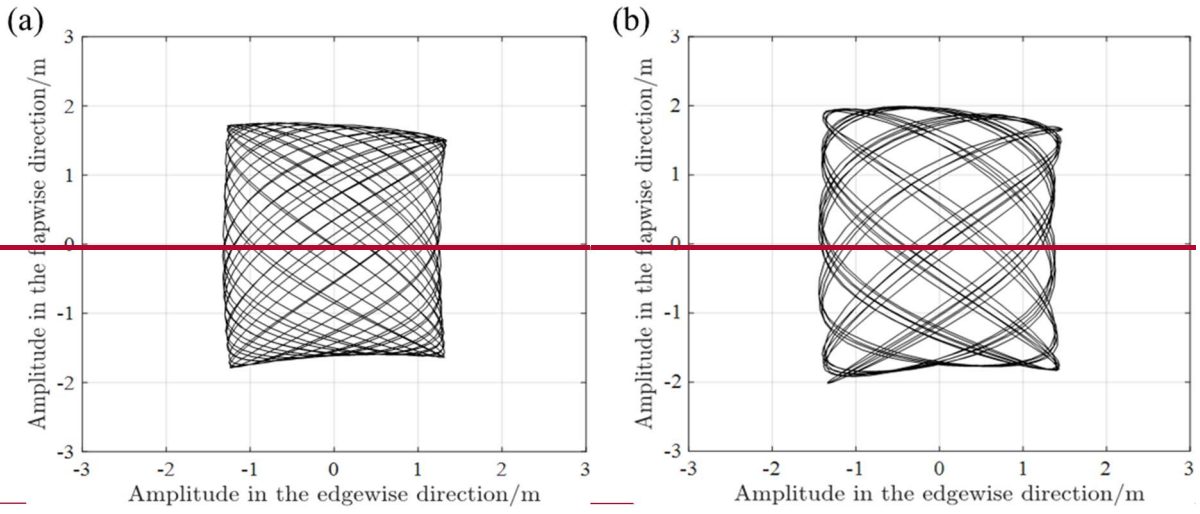


Figure 413: Biaxial trajectory of blade-virtual masses test system with same exciting force (at 63% of the blade position): (a)



**Natural frequency excitation (b) Resonance frequency excitation (Rotation) ; (c) Resonance frequency excitation (Actual Translation) ; (d) Resonance frequency excitation (Ideal Translation)**

**Table3. Biaxial excitation parameters of 94m**

<u>Virtual masses and exciting point</u>			<u>Natural frequency</u> [Hz]	<u>Sweep-frequency analysis</u>			
				<u>Uniaxial resonance frequency (Rotation)</u> [Hz]	<u>Biaxial resonance frequency</u> [Hz]		
<u>Position</u> [%]	<u>Force</u> [N]			<u>Rotation</u>	<u>Actual translation</u>	<u>Ideal translation</u>	
<u>Flap</u>	<u>63%</u>	<u>3800</u>	<u>0.377</u>	<u>0.373</u>	<u>0.369</u>	<u>0.375</u>	<u>0.377</u>
<u>Edge</u>	<u>52%</u>	<u>7000</u>	<u>0.589</u>	<u>0.587</u>	<u>0.583</u>	<u>0.587</u>	<u>0.589</u>

**Table4. Biaxial amplitude of 94m**

<u>Biaxial average amplitude [m]</u>			
	<u>Rotation</u>	<u>Actual translation</u>	<u>Ideal translation</u>
<u>Flap</u>	<u>1.923</u>	<u>2.113</u>	<u>2.154</u>
<u>Edge</u>	<u>1.447</u>	<u>1.511</u>	<u>1.630</u>

## 5 Conclusion

The nonlinear effect of virtual mass device on blade test system is discussed in this paper. In actual working conditions, the test system is limited by the size of the virtual mass mechanism and the amplitude of the blade, and its resonance characteristics will be changed. This paper firstly analyzed the nonlinearity of the system resonance characteristics from the mechanism of the change of the inertia force of the virtual mass, and established a blade uniaxial theoretical model to explore the influence of the amplitude of the blade and the size of the seesaw on the resonance frequency. Based on the above content, the approximate nonlinear amplitude-frequency characteristic curve of the test system is obtained. Then the software is used to simulate the two blades by the transient sweep method, and the applicability of the theoretical model is verified.

For the uniaxial theoretical model, the increase of blade amplitude, the shortening of seesaw size and the increase of counterweight mass will reduce the resonance frequency in the main vibration direction. However, the uniaxial simulation results of two blades show that the amplitude of the blade or the size of the seesaw have limited influence on the resonance frequency. For example, when the size of the mechanism is unchanged ( $L = R = 4m$ ), only the influence of blade amplitude on the system is considered. When the amplitude of the flapping direction increases to 2.6m, the resonance frequency in this direction decreases by nearly 2% compared with the natural frequency; Combined with the actual working conditions, when the amplitude of the flap-wise direction is maintained about 2m, the length of the seesaw is shortened to 3m, and the resonance frequency is reduced by nearly 2%. The target amplitude of the edge-wise is usually small compared with the flap-wise direction, so shortening the length of the seesaw only reduces the resonance frequency by 1.1%. In the case of the same amplitude, the shortening of seesaw length will reduce the blade load distribution level, and the flap-wise load level will decrease by up to 3% at most. Due to the small amplitude of the edge-wise, the load level in this direction does not drop

496 significantly.

497 Although the nonlinear factors have less influence on the uniaxial test, they have more influence on the biaxial test. Under  
498 the same excitation force and approximate target amplitude ( $Y \approx 2m$ ), the rotating virtual masses induces lower resonance  
499 frequency in biaxial vibration than in uniaxial test (Flap-wise direction: 1.06% decrease in uniaxial vibration, 2.12% decrease  
500 in biaxial vibration; Edge-wise direction: 0.34% decrease in uniaxial, 1.02% decrease in biaxial). In addition, under the same  
501 exciting force, the difference between the average flap amplitude of the blade using the rotating virtual mass mechanism and  
502 the average flap amplitude under the ideal condition is 9%, and the difference between the average edge amplitude and the  
503 average edge amplitude under the ideal condition is nearly 11%. Furthermore, the virtual masses mechanism can also cause  
504 the deformation of the space trajectory envelope of the blade. Under the combined action of many factors, the nonlinear effect  
505 will be further strengthened.

506 In conclusion, the virtual masses mechanism will bring nonlinear effect to the test system due to its own motion  
507 characteristics, and the nonlinear factors mainly include the amplitude of the blade, the size of the mechanism and the mass of  
508 the counterweight. In the case of small amplitude, the nonlinear effect is not obvious and has not great influence on the blade  
509 load level. In the biaxial large amplitude test, the nonlinear effect is enhanced and the blade trajectory is deformed. The  
510 resonance frequency of the system will be further reduced. Under the same excitation, the actual blade amplitude is less than  
511 the target amplitude. These characteristics mean that biaxial test requires larger excitation equipment and higher requirements  
512 for blade damage calculation and load formulation.

513 ~~This paper explores the effects of virtual masses device applied to blade biaxial fatigue test on the response characteristics of~~  
514 ~~the test system. Different from the additional masses directly installed on the blade, the nonlinearity of the test system originates~~  
515 ~~from kinematics of the virtual masses. Based on the analysis above, the main conclusions are shown as follows:~~

516 ~~1. The blade virtual masses test system shows nonlinear amplitude frequency characteristics. The square of the resonance~~  
517 ~~frequency is inversely proportional to the polynomial steady state response of the system. In the case of 80m blade, the~~  
518 ~~resonance frequency of the test system decreases by approximately 2% when amplitude is 2.6m during flap-wise vibration.~~

519 ~~2. The radius of the seesaw will also affect the vibration characteristics of the test system. The shorter the radius of the~~  
520 ~~seesaw, the stronger the nonlinear effects on the test system. When the blade flap amplitude is 2m and the radius is 3m, the~~  
521 ~~resonance frequency decreases by up to 1.8%. Due to the limited amplitude in the edge-wise direction, the radius of the seesaw~~  
522 ~~has minimal impact on the resonance frequency.~~

523 ~~3. The rotation radius of the seesaw will also affect the load distribution of the blade. Shortening the radius will reduce~~  
524 ~~the amplitude of blade load and the verification area of interest. The blade load distribution decreases by nearly 3% in the flap-~~  
525 ~~wise direction under the given operating conditions.~~

526 ~~4. When subjected to both large amplitude and short radius of the seesaw, the resonance frequency will decrease more~~  
527 ~~—significantly. It is important and necessary to consider the size and strength of the push rod and seesaw during practical~~  
528 ~~application. In addition to the influence on the resonance frequency and load distribution, the size and strength of the push rod~~  
529 ~~and seesaw also limit the maximum amplitude of the blade and the service life of the mechanism.~~

## 530 **References**

- 531 [1] Zhang, L. A. and Huang, X. M.: Study of wind turbine blade vibration characteristics under single point fatigue load  
532 driven. *Acta Energ. Sol. Sin. Acta Energiæ Solaris Sinica*, 36(05): 1112-1116, [https://doi.org/10.3969/j.issn.0254-](https://doi.org/10.3969/j.issn.0254-0096.2015.05.013)  
533 [0096.2015.05.013](https://doi.org/10.3969/j.issn.0254-0096.2015.05.013), 2015.
- 534 [2] Liao, G. H. and Wu, J. Z.: Wind turbine blade resonance fatigue loading system and experiment. *Acta Energ. Sol. Sin. Acta*  
535 *Energiæ Solaris Sinica*, 37(11): 2785-2791, <https://www.tynxb.org.cn/CN/Y2016/V37/I11/2785>  
536 <https://doi.org/10.19912/j.0254-0096.2016.11.009>, 2016.
- 537 [3] IEC: IEC 61400-23 – Wind Turbines Part 23: Full-scale Structural Testing of Rotor Blades, *International Electrotechnical*  
538 *Commission IEC*, Geneva, Switzerland, 2014.
- 539 [4] DNV GL AS: DNVGL-ST-0376 – Rotor blades for wind turbines, available at: [https://rules.dnvgl.com/docs/pdf/DNVGL/](https://rules.dnvgl.com/docs/pdf/DNVGL/ST/2015-12/DNVGL-ST-0376.pdf)  
540 [ST/2015-12/DNVGL-ST-0376.pdf](https://rules.dnvgl.com/docs/pdf/DNVGL/ST/2015-12/DNVGL-ST-0376.pdf) (last access: 7 June 2019), 2015.

- 541 [5] White, D.: New method for dual-axis fatigue testing of large wind turbine blades using resonance excitation and spectral  
542 loading, Tech. rep., National Renewable Energy Lab., Golden, CO, USA, <https://doi.org/10.2172/15007390>, 2004.
- 543 [6] Greaves, P. R., Dominy, R. G., Ingram, G. L., Long, H., and Court, R.: Evaluation of dual-axis fatigue testing of large  
544 wind turbine blades, P. I. Mech. Eng. C-J. Mec., 226, 1693–1704, <https://doi.org/10.1177/0954406211428013>, 2012.
- 545 [7] Snowberg, D., Dana, S., Hughes, S., and Berling, P.: Implementation of a Biaxial Resonant Fatigue Test Method on a  
546 Large Wind Turbine Blade, Tech. rep., National Renewable Energy ~~Lab.Laboratory~~, Golden, CO, USA,  
547 <https://doi.org/10.2172/1155105>, 2014.
- 548 [8] Hughes, S., Musial, W. D., and Stensland, T.: Implementation of a Two-Axis Servo-Hydraulic System for Full-Scale  
549 Fatigue Testing of Wind Turbine Blades, Tech. rep., National Renewable Energy ~~Lab.Laboratory~~, Golden, CO, USA,  
550 <https://www.osti.gov/servlets/purl/12200>, 1999.
- 551 [9] Liao, G. H. and Wu, J. Z.: Vibration Analysis of a Dual-axial Fatigue Loading System for Wind Turbine’s Blades Test.  
552 NOISE AND VIBRATION CONTROL, 34(05): 114-116, <https://doi.org/10.3969/j.issn.1006-1335.2014.05.026>, 2014.
- 553 [10] Post, N. and Bürkner, F.: Fatigue Test Design: Scenarios for Biaxial Fatigue Testing of a 60-Meter Wind Turbine Blade,  
554 Tech. rep., National Renewable Energy ~~Lab.Laboratory~~, Golden, CO, USA, <https://doi.org/10.2172/1271941>, 2016.
- 555 [11] Melcher, D., Bätge, M., and Neßlinger, S.: A novel rotor blade fatigue test setup with elliptical biaxial resonant excitation,  
556 ~~Wind Energy Sci.Wind Energ. Sci~~, 5(2): 675-684, <https://doi.org/10.5194/wes-5-675-2020>, 2020a.
- 557 [12] Melcher, D., Petersen, E., and Neßlinger, S.: Off-axis loading in rotor blade fatigue tests with elliptical biaxial resonant  
558 excitation, ~~J. Phys.: Conf. Ser.J. Phys. Conf. Ser~~, 1618(5): 052010, <https://doi.org/10.1088/1742-6596/1618/5/052010>,  
559 2020b.
- 560 [13] Lu, L., Zhu, M., and Wu, H.: A Review and Case Analysis on Biaxial Synchronous Loading Technology and Fast  
561 Moment-Matching Methods for Fatigue Tests of Wind Turbine Blades. ENERGIES, 15(13) :4881,  
562 <https://doi.org/10.3390/en15134881>, 2022.
- 563 [14] Zhang, J. B., Shi, K. Z., and Zhang, C. Y.: Improving accuracy of dual-axial resonance fatigue testing for wind turbine  
564 blades by using predicted equivalent test loads caused by combined loading, J. Renew. Sustain. Energ., 12(1):013303,  
565 <https://doi.org/10.1063/1.5112006>, 2020.
- 566 [15] Castro, O., Belloni, F., and Stolpe, M.: Optimized method for multi-axial fatigue testing of wind turbine blades, Compos.  
567 Struct., 257: 113358, <https://doi.org/10.1016/j.compstruct.2020.113358>, 2021.
- 568 [16] Melcher, D., Rosemann, H., and Haller, B.: Proof of concept: elliptical biaxial rotor blade fatigue test with resonant  
569 excitation, IOP Conf. Series: Mat. Sc. and Eng., 942(1): 012007, <https://doi.org/10.1088/1757-899X/942/1/012007>,  
570 2020c.
- 571 ~~[17]~~ Falko, B.: Biaxial Dynamic Fatigue Tests of Wind Turbine Blades, Ph.D. thesis, Leibniz University Hannover, Germany,  
572 <https://publica.fraunhofer.de/handle/publica/283519>, 2020.
- 573 ~~[18]~~ Liu, Y. Z., Chen, L. Q., and Chen, W. L.: ~~Mechanics of Vibration, Higher Education Press,~~  
574 <https://xuanshu.hep.com.cn/front/book/findBookDetails?bookId=5bed82d7f18f967ee7f37a8a>, 2019.
- 575 ~~[19]~~ Liu, Y. Z., Chen, L. Q.: ~~Nonlinear vibrations, Higher Education Press,~~ <https://www.dushu.com/book/10052149/>, 2001.
- 576 ~~[17]~~~~[20]~~ LEE, H. G., LEE, J.: ~~Damping mechanism model for fatigue testing of a full-scale composite wind turbine blade,~~  
577 ~~Part 1: Modeling, Compos. Struct., 202: 1216-1228,~~ <https://doi.org/10.1016/j.compstruct.2018.05.124>, 2018.
- 578

## 579 Code and data availability.

580 The data that support the findings of this research are not publicly available due to confidentiality constraints.

## 581 Author contributions.

582 JS conceptualized and defined the requirements for the method developed. AZ supervised the work. JS and TD developed

583 the model code and performed the simulations. JS prepared the manuscript with contributions from all co-authors.

584 **Competing interests.**

585 The authors declare that they have no conflict of interest.

586 **Financial support.**

587 Blade data of this research has been supported by Aeolon Technology Co., L

588